The luminescent and photophysical properties of covalent organic frameworks

W. Karl Haug, [ID] † Erica M. Moscarello, [ID] † Eric R. Wolfson [ID] † and Psaras L. McGrier [ID] *

Covalent organic frameworks (COFs) are an emerging class of crystalline porous polymers that have attracted significant attention due to their tunable properties and structural robustness. As a result, COFs with luminescent properties are of great interest for fields such as chemical sensing, solid-state light emitters, photocatalysis, and optoelectronics. However, the bottom-up synthesis of luminescent COF systems remains a challenge in the field due to an abundance of competing non-radiative pathways, including phenomena such as aggregate caused quenching (ACQ). To overcome these obstacles, there has been a burgeoning investigation into the luminescent and photophysical properties of COFs. This review will highlight methods used to fabricate luminescent COFs and discuss the factors that are critical for their production. A collection of known luminescent COF systems will be featured. In addition, the ability to utilize the photophysical properties of COFs for applications related to photocatalysis, solid-state light emitters, and chemical sensing will be addressed. An outlook will address the current progress and remaining challenges facing the field to ultimately expand the scope of their applications.

1. Introduction

Light is essential for life on earth. The investigation of light and light-emitting processes has long been of interest to society, resulting in significant advances in modern technology such as light-emitting diodes (LEDs),[1,2] photography,[3] and forensics.[4] Photoluminescence (PL) is a phenomenon wherein a photon is absorbed by a chromophore through a photoexcitation event,

Department of Chemistry & Biochemistry, The Ohio State University, Columbus, Ohio 43210, USA. E-mail: mcgrier.1@osu.edu

† W. K. H., E. M. M., and E. R. W. contributed equally to this review.

followed by photon emission as a consequence of electron relaxation. However, there are a number of different pathways through which a photoexcited state can return to its ground state. These relaxation pathways may be as fast as 10^{-12} s,[5] or as slow as hours,[6] depending on the photophysical properties of the chromophore. Radiation from a transition between states of the same multiplicity (*i.e.*, $S_1 \rightarrow S_0 + h\nu$) is referred to as fluorescence. In some instances, the excited electron can undergo a spin–flip. This intersystem-crossing (ISC) event can produce a longer-lived photon emission process, in a phenomenon known as phosphorescence. This longer lifetime of emission, or afterglow, can be attributed to the 'forbidden'

W. Karl Haug is a PhD candidate advised by Psaras L. McGrier at The Ohio State University. He received his bachelor's degree from University of Denver in 2016 where he worked on photo-induced cyclizations of ortho-oxaxylylenes, in the lab of Andrei Kutateladze. His current research interests are focused on the utilization of metal-doped covalent organic frameworks as a platform for heterogeneous catalysis.

W. Karl Haug

Erica Moscarello received her BS from Rowan University in 2017 where she worked under the supervision of Professor Gustavo Moura-Letts. She is currently in the third year of her PhD at The Ohio State University under the supervision of Professor Psaras McGrier. As a doctoral student, her work focuses on investigating the thermal properties of benzo-bisoxazole-linked covalent organic frameworks.

Erica M. Moscarello

nature of the transition from the meta-stable triplet state to the singlet ground state (*i.e.*, $T_1 \rightarrow S_0 + h\nu$). The continued investigation of photophysical properties is paramount to the development of more advanced technologies, and therefore society as a whole.

The examination and practical use of luminescent polymers has seen a recent boom due to the development of advanced materials such as hyper-crosslinked polymers (HCPs),[7,8] polymers of intrinsic microporosity (PIMs),[9] porous organic polymers,[10–13] π-conjugated polymers,[14] and metal organic frameworks (MOFs).[15,16] In particular, the advancement of luminescent porous materials has been largely due to (a) the ability to incorporate fluorescent probes directly into the polymer skeleton, (b) the tunability of optoelectronic properties through careful selection of monomers, and (c) a growing interest in heterogeneous sensors which can be used repeatedly without loss of activity or contamination of the sample. As a direct result of this research, significant advances in fields such as chemical sensing,[17–19] organic light emitting polymers,[20–22] and phototherapy[23–26] have been made. However, due to the often-amorphous nature of these materials, fluorescent polymers can be challenged by poor solvent permeability leading to decreased sensitivities. In addition, in the case of MOFs, high densities and poor hydrolytic stabilities are major issues challenging their use in commercial applications. There is an ongoing need for the further development of novel, stable, and highly performing luminescent materials that can be processed into a variety of forms while still retaining their desired photophysical properties and activity.

Covalent organic frameworks (COFs)[27–29] are an advanced class of crystalline porous polymers that enable the integration of various molecular building blocks into highly ordered periodic arrays. The modular nature of COFs has made them of immense interest in a variety of applications including energy storage,[30,31] catalysis,[32,33] gas storage,[34] and carbon capture.[35] A large portion of COF research has been focused on developing methods to incorporate novel linkages and building blocks, allowing for COFs with different functional architectures.[36] A large area of research has since been focused on working towards utilizing these innovative materials and their unique properties in different applications. One such area of research focuses on exploiting the photophysical properties of COFs. COFs that exhibit tunable photophysical properties are particularly desirable for applications in chemical sensing,[37] photocatalysis,[38] and organic light emitting diodes (OLEDs).[39] The interactions between the monomer units and adjacent layers of COFs can greatly influence their photophysical properties, giving them a distinct advantage over amorphous materials with the same components. Therefore, it is important to understand the underlying principles that govern the luminescent properties of these materials.

The following review will discuss COFs in the context of their luminescent and photophysical properties. Specifically, this review will include a summary of methods used to fabricate luminescent COFs, a collection of known luminescent COF systems, and a discussion about the factors that are critical for producing luminescent COFs. In addition, the use of COFs for applications related to chemical sensing, photocatalysis, as well as light emitters and photodetectors will also be addressed.

2. COF synthesis and design

Initially, COFs were primarily designed utilizing dynamic covalent chemistry in conjunction with favorable non-covalent
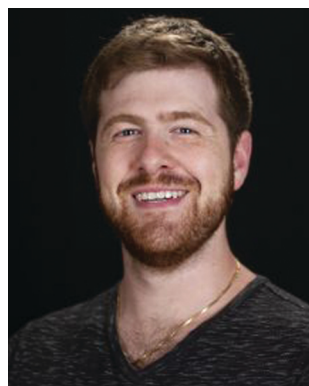
Eric Wolfson received his bachelor's degree in Chemistry in 2015 from University of Maryland Baltimore County, where he studied the cure kinetics of fast-setting epoxy resins under Dr Lisa Kelly. Eric also worked on the synthesis of CdSe and PbSe nanowires under Dr Narsingh Singh. He has conducted his PhD research under the guidance of Psaras McGrier since 2016 at The Ohio State University. As a doctoral student, his work focuses on functional porous organic polymers for use as cutting-edge energy storage materials.

Eric R. Wolfson

Psaras is an Assistant professor in the Department of Chemistry and Biochemistry at The Ohio State University. He received his BS in Chemistry from the University of South Carolina-Aiken in 2004 and his PhD in Organic/Polymer chemistry from the Georgia Institute of Technology (Georgia Tech) in 2010 under the direction of Professor Uwe Bunz. After finishing his PhD, he moved to Northwestern University (2010– 2013) to join the group of Professor Sir Fraser Stoddart as a postdoctoral scholar on a fellowship from Georgia Tech Facilitating Academic Careers in Engineering and Science (FACES) committee and the National Science Foundation (NSF). His current research interests include the synthesis and utilization of 2D and 3D porous polymers for practical applications. He is a recipient of the 2018 ACS Division of Polymeric Materials: Science and Engineering (PMSE) Young Investigator Award.
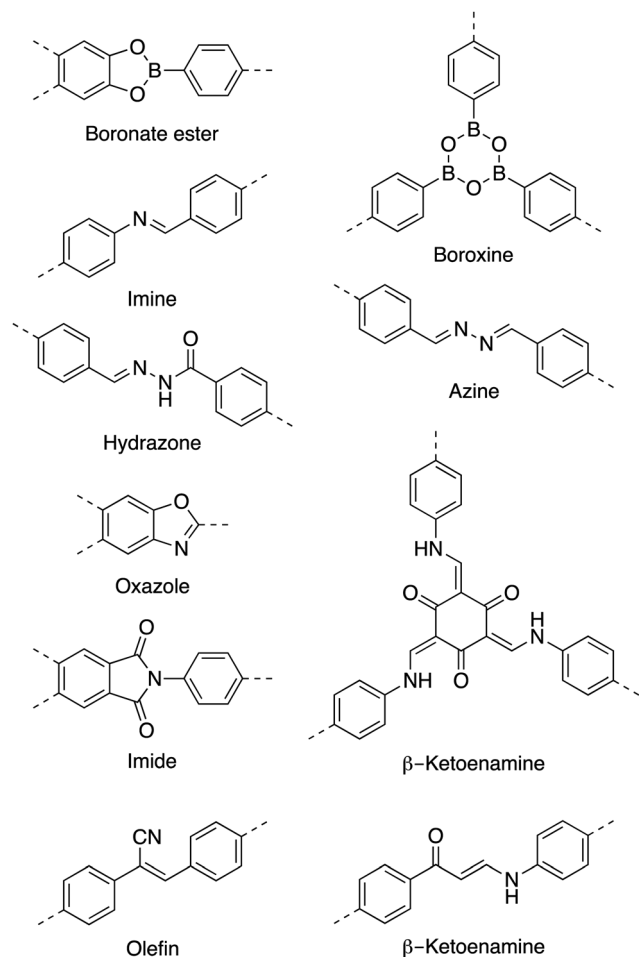
Psaras L. McGrier

Chart 1 Common linkages used in COFs.

interactions to form ordered and permanently porous materials. In 2005, Yaghi and co-workers utilized the high reversibility of boroxine and boronate ester condensation reactions to develop the first COFs.[27] However, these linkages exhibited weak hydrolytic stability. The challenge to synthesize more robust frameworks using different connectivities soon led to the development of more chemically stable linkages such as imines,[40] oxazoles,[35,41] and olefins[42] (Chart 1).

As a result of using only organic building blocks and covalent linkages, COFs are also often characterized as having low densities and high thermal stabilities.[29] By selecting π-electron rich monomers with specific symmetries, a variety of 2D and 3D[43,44] architectures have been achieved (Fig. 1).[45] This strategy not only allows one to have precise control over the topology of the material, but also allows for the ability to pre-tailor bulk properties and performance for specific applications through the careful choice of suitable monomers (Chart 2). In addition, the ability to incorporate functional moieties that remain inert during COF synthesis allows one to further post-functionalize the molecular skeleton. As a consequence, these design strategies have enabled the creation of various functional COFs with a high degree of tunability.
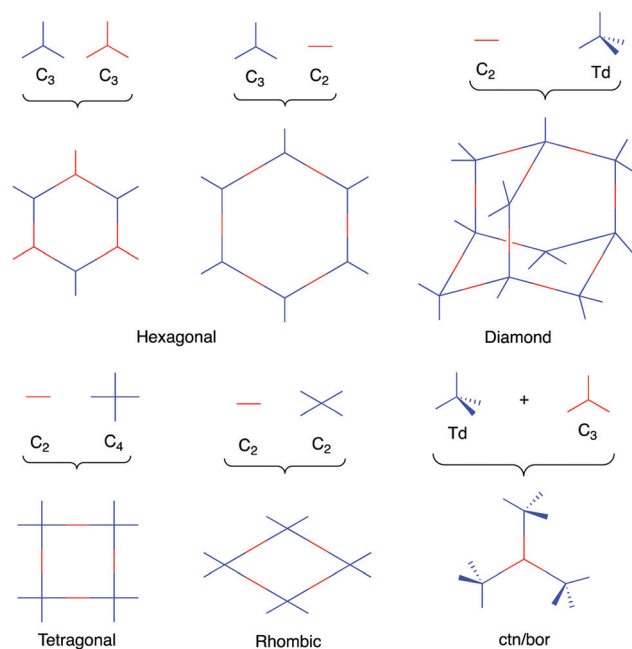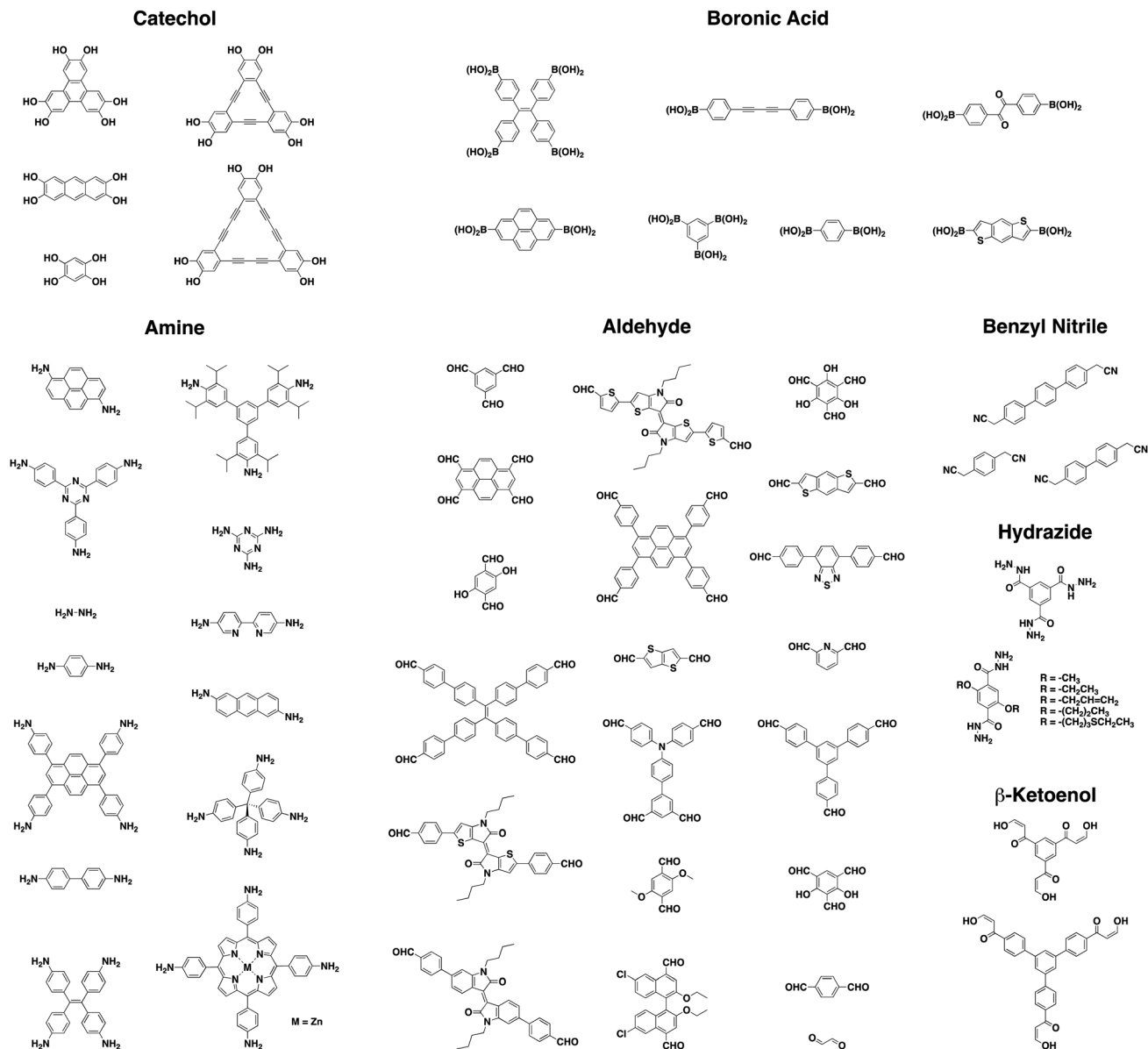

Fig. 1 Sample of topologies accessible through COF synthesis.

Initially, solvothermal methods were utilized in the synthesis of COFs. The use of high temperatures in a closed system promotes reversibility and eventually drives product formation towards the thermodynamically favored product. Due to the poor solubility of COF crystallites in solution, the solvothermal method typically limits applications to those where a bulk powder is sufficient. As a result, a key challenge is improving the scalability and processability of COF materials. Interest in expanding the scope of COF-based applications has led to methodologies such as mechanochemical, microwave, ionothermal, and substrate-templated synthesis.[45] As a result, COFs have now been processed into a variety of forms including nanoparticles, hollow microspheres/rods, and membranes.[46,47] A number of these forms such as thin films and exfoliated sheets have yielded materials suitable for photoluminescent applications.[32]

While new and more robust linkages led to substantial progress in the development of new COF systems, the polymerization and crystallization processes remained poorly controlled during their syntheses. COFs are predominantly formed as polycrystalline aggregates with small crystalline domains, and a major hurdle in the synthesis of more crystalline materials was a poor fundamental understanding of nucleation and crystallite growth processes. Therefore, it was of great interest to develop and investigate synthetic methods that yield single-crystalline COFs. As a result, single-crystalline COFs with 3D[48] and 2D[49] topologies have been successfully developed via the use of modulators and directed growth, respectively. In addition, mechanistic investigation of COF 5[50] formation led to new insights on the impact of reversible bond formation. Dichtel and co-workers eventually utilized this new information to form single-crystalline COFs via a seeded-growth method.[51]

This journal is © The Royal Society of Chemistry 2020

Chem. Soc. Rev., 2020, 49, 839–864 | 841

Chart 2 Examples of monomers used in luminescent COFs referenced in this review.

To control the orientation of growth, extensive research has been dedicated to growing COFs as oriented thin films.[52–56] This often leads to a more uniform material with less defects allowing for the study of anisotropic properties. Additionally, this processing method results in materials viable for a larger range of applications where bulk powder is not sufficient. Dichtel and co-workers reported the growth of a crystalline covalent organic film on a substrate-supported single layer graphene in 2011.[57] Bein and co-workers have also made significant contributions towards advancing the field both in the fabrication of thin films as well as their utilization in applications.[58–60] It was initially believed that favorable π-interactions between the substrate surface and COF monomers was necessary for successful COF thin film growth. Bein and co-workers showed that this was not necessarily true by growing thin films of a benzodithiophene COF (BDT-COF)

on multiple polycrystalline inorganic substrates including indium-doped tin oxide substrates, gold surfaces, and fused silica substrates.[61]

3. Origins of luminescence in COFs

3.1. Extended conjugation

It is well understood that π-systems undergo electronic excitations more easily than their saturated counterparts.[62] This is due to the lower energy difference (ΔE) for a π–π* transition than for a σ–σ* transition, thus leading to a higher λ_{max}. This effect is enhanced for conjugated systems where the π–π* transitions are redshifted to longer wavelengths (lower ΔE).

842 | *Chem. Soc. Rev.*, 2020, **49**, 839–864

This journal is © The Royal Society of Chemistry 2020

Yoshida and co-workers were able to establish a relationship between the length of π-conjugation and fluorescence emission efficiency of a system by comparing fluorescent quantum yields (Φ_f), and other photophysical properties (λ_{em}, λ_{abs}), to the π-structure of common fluorophores.[63] Their results demonstrated a nearly linear relationship between Φ_f (for $0.1 > \Phi_f > 0.9$) and the magnitude of π-conjugation length (A_π) in the S_1 state of the investigated hydrocarbon fluorophores. Additionally, it was revealed that a positive linear relationship between A_π and λ_{em} exists for linear oliogophenylenes. This discovery highlighted how extending the conjugation of chromophores can significantly affect their luminescent properties.

1D polymers have taken advantage of extended conjugation for applications including photovoltaics, sensors, field-effect transistors, photodetectors, and organic light-emitting diodes.[64] The ability to further propagate π-conjugation in two spatial directions has the potential to greatly improve upon the abilities and functions of these materials. 2D COFs present an ideal platform to achieve this goal, as their planar sheets have the potential to extend π-conjugation in multiple directions, while their modular nature allows for the precise placement of functional units within the framework.

In an effective demonstration of the influence that extended conjugation has on 2D COFs, Jiang and co-workers incorporated conjugated anthracene units into Ph-An-COF,[65] yielding a fluorescent system (λ_{em} = 429 nm, Φ_f = 5.4%). Due to the AA-stacking of the COF layers, the photoactive anthracene units were aligned in a face-on-face π-stacking pattern with an intermolecular (interlayer) distance of 3.4 Å. The proximity (>4 Å) and alignment of the π-stacked anthracene units allowed for their photo-induced dimerization (Fig. 2). Upon irradiation under Ar (xenon lamp, 360 nm light), the newly formed Ph-An$_{CD}$-COF displayed quenching of the material's

fluorescence. The significant change in the photophysical properties of the COF can be attributed to the loss of planarity and extended π-conjugation within the 2D layers upon the formation of the anthracene dimers. It was further demonstrated that the fluorescence could be regained when the anthracene units were returned to their planar state via the thermally-reversible cycloaddition.

In an attempt to increase the extent of π-conjugation throughout the layers in 2D-COFs, Perepichka and co-workers developed a novel linkage by taking advantage of the reversibility of Michael addition–elimination reactions.[66] Several chemically stable and ordered frameworks were achieved through the condensation of various β-ketoenols and aromatic amines. The resulting COFs were linked through β-ketoenamine functionalities. This linkage strategy demonstrated improved chemical stability as compared to their imine-linked counterparts, while simultaneously providing extended conjugation in the system. The effects of the π-conjugation could be observed as an orange, solid-state luminescence (λ_{max} = 547–560 nm) which was redshifted from that of the reference compounds (λ_{max} = 480–510 nm).

3.1.1. Fully sp²-carbon-linked COFs. Imine linkages are capable of propagating extended π-conjugation through the C=N bonds. However, these linkages often lead to relatively weak electron delocalization due to the high polarization of the C=N bonds.[66] Switching from Schiff base to Knoevenagel condensations allows for the synthesis of olefin (C=C) linked COFs.[67–71] These olefin linkages not only allow for significant enhancements in chemical stability, but also increase the effectiveness of π-conjugation between monomer units in the fully sp²-carbon-linked 2D systems.

When Li and co-workers employed a Knoevenagel condensation between 2,4,6-tris(4-formylphenyl)-1,3,5-triazine (TFPT) and 2,2′-(1,4-phenylene)diacetonitrile (PDAN), a fully conjugated 2D sp²-carbon linked COF (TP-COF) was obtained.[70] TP-COF was isolated as a yellow crystalline solid that exhibited bright solid-state fluorescence (λ_{em} = 543 nm). The observed solid-state fluorescence for TP-COF showed a noticeable redshift (37 nm) when compared to the synthesized model compound (λ_{em} = 506 nm) (Fig. 3). This shift towards a longer wavelength was attributed to the successful synthesis of an extended π-conjugated framework.
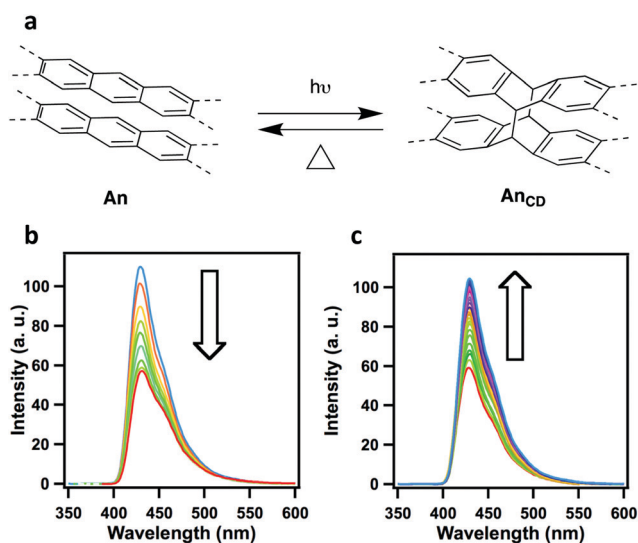

Fig. 2 (a) Photo-induced and thermally reversible dimerization of anthracene units. Changes in the fluorescence spectra of (b) Ph-An-COF upon photoirradiation, and (c) recovery of Ph-An-COF from the heating of Ph-An$_{CD}$-COF, 100 °C in the dark. Adapted with permission from *Angew. Chem., Int. Ed.*, 2015, **54**, 8704–8707.
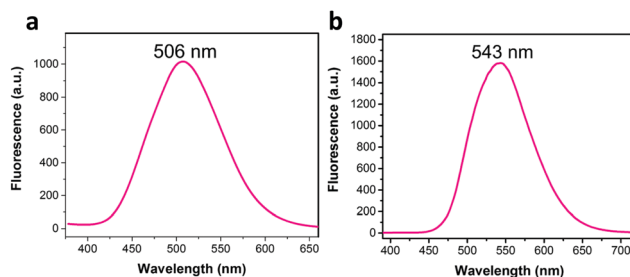

Fig. 3 The 37 nm redshift in solid-state fluorescence spectra of (a) the model compound, and (b) TP-COF. Adapted with permission from *Angew. Chem., Int. Ed.*, 2019, **58**, 5376–5381.
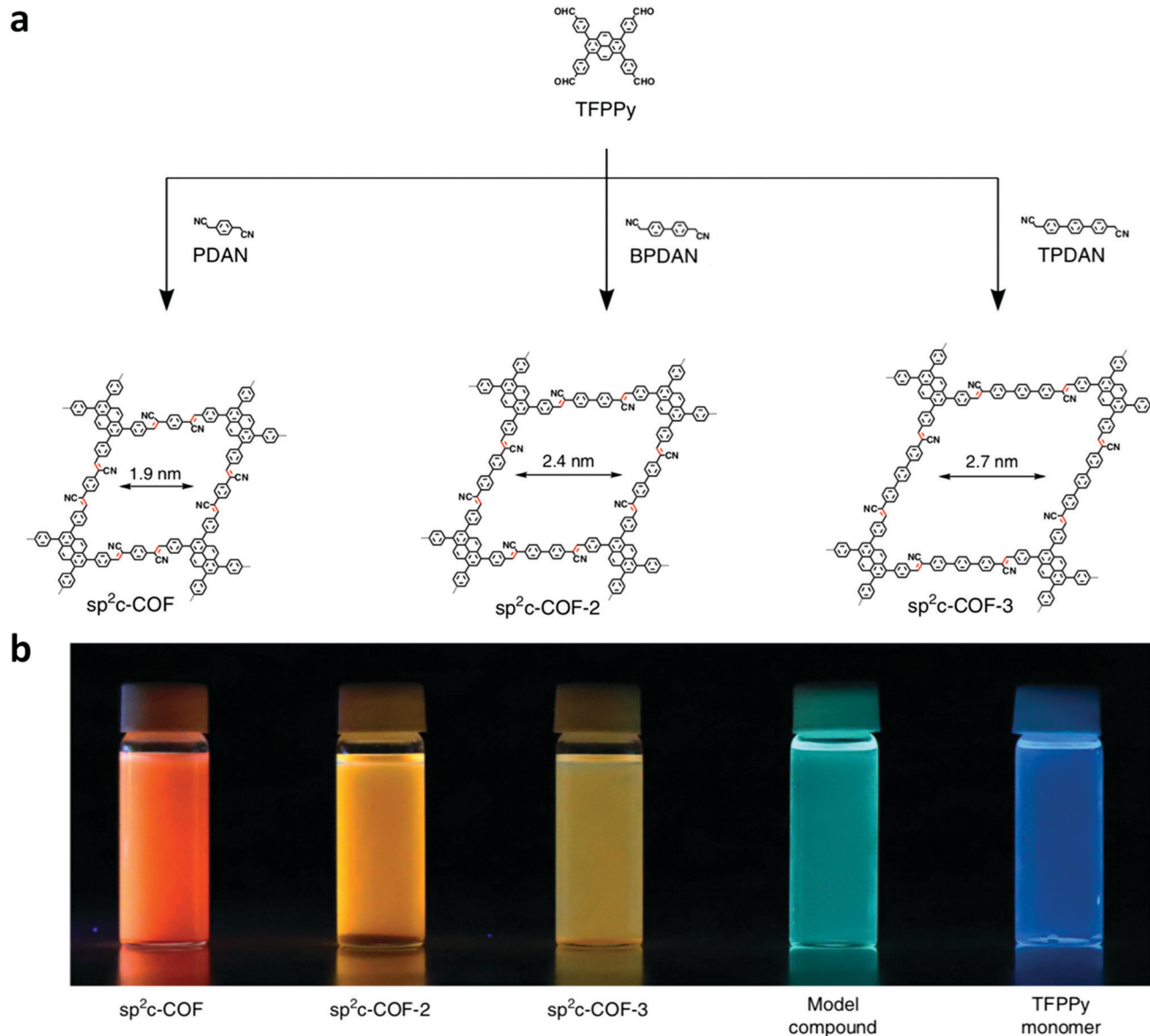
a

b

Fig. 4   (a) Design and structures of sp^{2}c-COFs from the condensation of TFPPy with PDAN, BPDAN, and TPDAN. (b) Images of sp^{2}c-COF, sp^{2}c-COF-2, sp^{2}c-COF-3, model compound, and TFPPy monomer dispersed in water under a UV lamp. Adapted with permission from *Nat. Commun.*, 2018, **9**, 4143.

Jiang and co-workers were able to synthesize a series of sp^2 carbon-conjugated 2D-COFs (sp^{2}c-COFs) through the condensation between a tetraphenylpyrene aldehyde unit and linear C_2-symmetric phenyl diacetonitrile linkers (Fig. 4).[71] Each sp^{2}c-COF was fluorescent and exhibited linker-dependent emission colors. The extent of the π-conjugation derived from the incorporation of olefin linkages was investigated by comparing the electronic absorption bands of sp^{2}c-COF, the synthesized model compound, and an imine-linked pyrene COF with a similar skeleton to sp^{2}c-COF (Fig. 4b). As expected, when compared to the synthesized model compound, sp^{2}c-COF exhibited a large (53 nm) redshift. When the imine-linked version of sp^{2}c-COF was investigated, it only showed a redshift of 21 nm compared to the model compound. This larger bathochromic shift in the sp^{2}c-COF demonstrated that the

C=C linkage is much more effective than the C=N linkage at creating an extended π-conjugated framework. Although both sp^{2}c-COF-2 and sp^{2}c-COF-3 exhibited redshifts when compared to the model compound, they were blueshifted from sp^{2}c-COF by 17 and 36 nm, respectively. These hypochromic shifts were associated with lessened efficiency of π-conjugation throughout the framework, caused by the twisted nature of the biphenyl and terphenyl moieties disrupting the π-conjugation. The twisted structures of sp^{2}c-COF-2 and sp^{2}c-COF-3 could also be observed through their increased interlayer separation distances (3.74 and 3.79 Å compared to 3.58 Å for sp^{2}c-COF). In addition to tuning the λ_{abs}, the switching of linkers also led to a change in the structure's band gap. As the efficiency of π-conjugation decreased, the band gap increased.

3.2. Excited-state intramolecular proton transfer

Excited-state intramolecular proton transfer (ESIPT) is a photochemical process that can be utilized to construct luminescent materials. This photoinduced process has been exploited and investigated for numerous applications[72–74] since it was first reported by Weller in 1955.[75] ESIPT is a phototautomerization that occurs when a chromophore contains an intramolecular hydrogen bond donor (–OH, –NH₂) and a hydrogen bond acceptor (–C=O, –C=N–) in close proximity. Upon photoexcitation, many systems exhibit dual emission bands that encompass the entire visible spectrum due to the rapid four-step enol (E–E*)–keto (K–K*) phototautomerization process (Fig. 5). This four-step photochemical process has proven to be beneficial for sensory-based applications.

In 2017, Yan and co-workers developed TzDa, a highly crystalline COF with dual emissions to detect trace water in organic solvents.[76] 4,4′,4″-(1,3,5-Triazine-2,4,6-triyl)trianiline (Tz) and 2,5-dihydroxyterephthalaldehyde (Da) were chosen as monomers, to incorporate both an intramolecular charge transfer (ICT) and an ESIPT moiety, respectively, into the polymeric system. The investigation of the effect of water in these two processes enabled the success of the ratiometric fluorescent sensor. The increase of water content was observed to lead to a higher fluorescence intensity of the longer wavelength emission and a reduction in intensity of the shorter wavelength emission. It was hypothesized that this result arose from the interference of water on the COF's intramolecular processes. The docking of a water molecule on the Tz moiety prevented the ICT process from the triazine to the phenyl group from taking place. Similarly, the interaction of water molecules with the –OH group on the Da moiety led to the interruption of intramolecular hydrogen bonding (Fig. 6). The synergetic effect
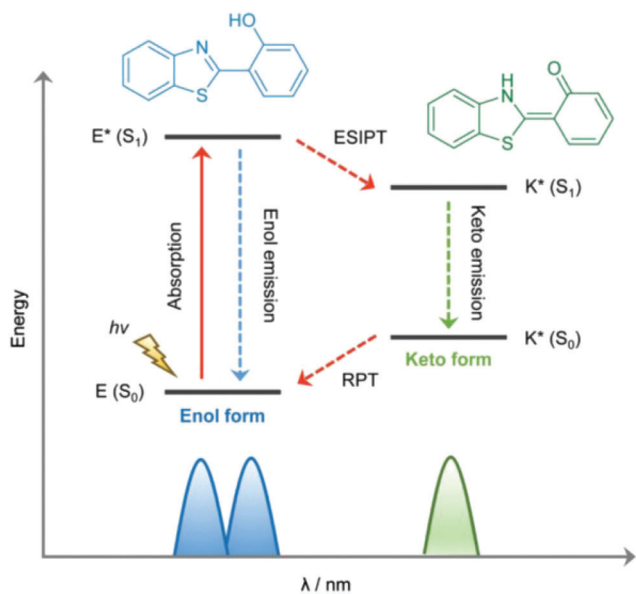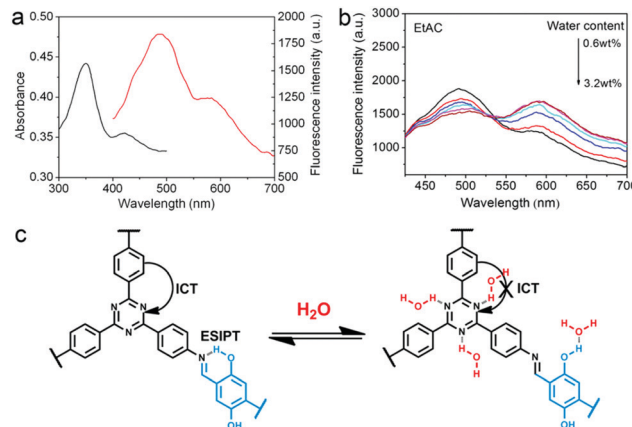
Fig. 6 (a) Absorption (black) and fluorescence (red) spectra of TzDa in EtOAc. (b) Ratiometric fluorescence sensing of TzDa in EtOAc with varying water content. (c) Interruption of intramolecular hydrogen bonding in TzDa upon introduction of water. Reprinted with permission from *ACS Appl. Mater. Interfaces*, 2017, **9**, 24999–25005. Copyright 2017 American Chemical Society.

resulted in the intensity changes of both emission peaks and ultimately the detection of trace water in organic solvents.

Vaidhyanathan and co-workers developed an anthracene-resorcinol-based COF that exhibited white-light emission.[77] IISERP-COF7 was synthesized as a black powder that emitted white light when dispersed in *N*-methylpyrrolidone (NMP). Upon excitation at 340 nm, the emission spectrum exhibited three bands corresponding to blue, green, and red. It was hypothesized that the green and red light were both originating from the resorcinol trialdehyde unit. This unit exhibits yellow light under UV, which lies between red and green on the color map. Keto–enol tautomerization was expected between the resorcinol trialdehyde and anthracene unit due to the geometry between the two moieties connected *via* an imine bond. The color of the IISERP-COF7 could be manipulated through dispersion in different solvents. By utilizing O- or N-donating solvents, the intensity of the blue-green or yellow-orange band, respectively, could be increased. O-Donating solvents stabilized the enol form *via* hydrogen bonding, effectively increasing the intensity of the blue-green band. N-Donating solvents stabilized the keto form by acting as a base to assist in the transfer of the enol proton to the nitrogen, resulting in the increase in intensity of the yellow-orange band. NMP contains both an oxygen and basic nitrogen and was therefore found to stabilize both forms, resulting in near-white-light emission (Fig. 7). UV-vis spectra were taken of the IISERP-COF7 dispersed in aprotic toluene and protic ethanol. No new bands appeared due to any potential intermolecular proton transfer between solvent molecules and the COF, indicating the presence of an ESIPT process.

3.3. Aggregation induced emission

In a highly fluorescent system, radiative decay outcompetes the many non-radiative pathways available. However, for some systems, steric and/or electronic interactions inhibit radiative decay while solvated. In some of these cases, it is possible to

Fig. 5 Mechanistic representation of excited state intramolecular proton transfer. Reproduced from *Chem. Soc. Rev.* 2018, **47**, 8842–8880, with permission from the Royal Society of Chemistry.
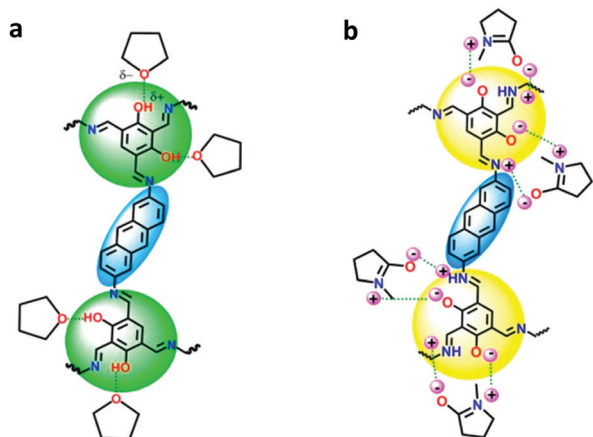
Fig. 7 (a) Stabilization of the enol-form due to hydrogen bonding by THF. (b) Stabilization of the intermediate keto–enol form by the polarized NMP. Adapted with permission from *J. Am. Chem. Soc.*, 2018, **140**, 13367. Copyright 2018 American Chemical Society.

sequester the faster, non-radiative pathways *via* aggregation. This aggregation allows the radiative decay processes to compete effectively, and thus improves the emission quantum yield. This aggregate-induced emission (AIE) process can be attributed to various factors such as reduced intramolecular rotations (RIR), reduced intramolecular vibrations (RIV), and reduced intramolecular motions (RIM).[78]

3.3.1. Tetraphenylethene-based COFs. The use of tetra-phenylethene (TPE) as a monomer has attracted much attention as an AIE luminogen (AIEgen) due to its strong RIR-induced emission. TPE was utilized as a monomer for a fluorescent COF system by Jiang and co-workers in 2016.[79] The co-condensation of a TPE-cored boronic acid (TPEBA) with 1,2,4,5-tetrahydroxy-benzene (THB) formed the fluorescent TPE-Ph COF (Fig. 8).

The polymer crystallized in a Kagome lattice with AA stacking and demonstrated a fluorescence quantum yield of 32%, which was noted as the highest fluorescence quantum yield for a COF to that point. This value is notably enhanced compared to its small-molecule analog (Φ_f = 15%), owing to significant rotational restrictions (216.7 kcal mol^{-1}) imparted on the TPE vertices by the layered structure of the material.

In 2018, Wang and co-workers synthesized a 3D imine-linked COF, 3D-TPE-COF, which adopted a 7-fold interpene-trated unit-cell.[39] The COF's photoluminescence quantum yield (Φ_{PL} = 20%) was markedly higher than its model compound (Φ_{PL} = 6.6%), which was ascribed to both the rotational and vibrational relaxations being restricted when packed in the COF structure.

Zhao and co-workers investigated the AIE characteristics of TPE with regard to extended structures.[80] When aniline was condensed with an aldehyde-functionalized TPE unit (TFBE) to form the small molecule TMBE, the fluorescence enhancement was greatly reduced compared to free TFBE. Specifically, when comparing their fluorescence intensities in a 90:10 H$_2$O/THF mixture *versus* in pure THF, TFPE's enhancement ratio was ∼164; however, TMBE demonstrated only a 4.4-fold increase (Fig. 9b). This was attributed to TMBE's inability to planarize due to steric effects with its neighboring phenyl groups. By conformationally locking the COF system both laterally and vertically, it was thought that the AIE masking could be enhanced (Fig. 9c). Thus, azine-linked NUS-30, imine-linked NUS-32, and mixed imine/azine-linked NUS-31 were synthe-sized through condensation of an aldehyde-functionalized TPE with either hydrazine, 1,4-diaminobenzene, or a 1:1 ratio of each, respectively, which were then processed into nanosheets. All three polymeric systems showed almost complete AIE suppression with fluorescence enhancements of only
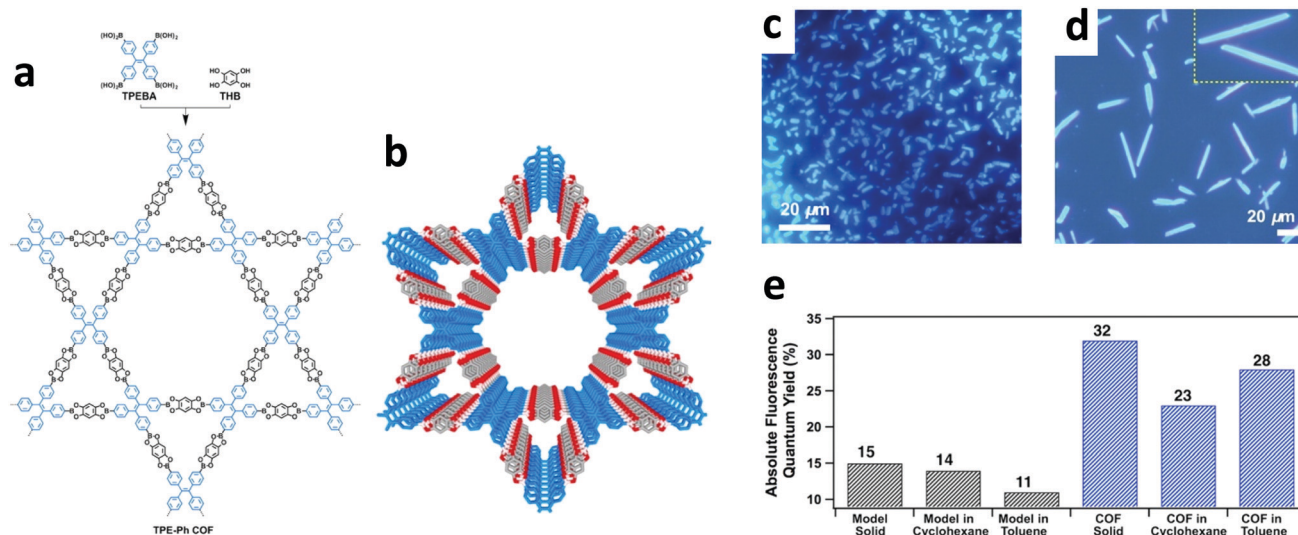

Fig. 8 (a) Synthesis of TPE-Ph COF from the condensation of TPEBA and THB. (b) Crystal structure of TPE-Ph COF with AA stacking mode. Fluorescence microscopy images of TPE-Ph COF samples synthesized in (c) 3 days (d) 30 days (the yellow insert depicts an enlarged view of the belts). (e) Comparative fluorescence quantum yields of TPE-Ph COF and the model compound dispersed in cyclohexane and toluene, as well as in the solid state. Adapted with permission from *J. Am. Chem. Soc.*, 2016, **138**, 5797–5800. Copyright 2016 American Chemical Society.

846 | *Chem. Soc. Rev.*, 2020, **49**, 839–864
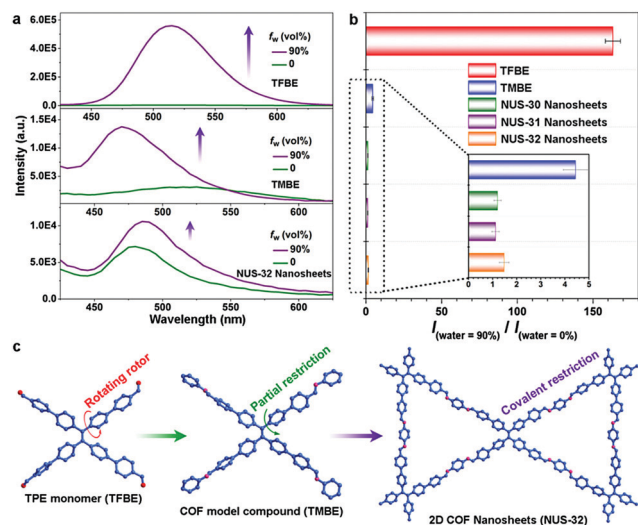
This journal is © The Royal Society of Chemistry 2020

Fig. 9 (a) Fluorescence spectra (λ_{ex} = 365 nm) of TFBE, TMBE, and NUS-32 in dry solvent or 90% water fractions. (b) Relative fluorescence intensities of TFBE, TMBE, and NUS 30–32 in solvent/water mixtures compared to dry solvent [I(water = 90%)/I(water = 0%)]. (c) Representation of the increasing restriction of AIE molecular rotor from monomer (TFBE) to COF model compound (TMBE) to 2D COF nanosheets (NUS-32). Reprinted with permission from *Chem. Mater.*, 2019, **31**, 146–160. Copyright 2019 American Chemical Society.

1.2-, 1.1-, and 1.5-fold for NUS-30, NUS-31, and NUS-32, respectively. Additionally, when suspended in 90:10 water/MeCN solutions, a bathochromic shift was observed for all three nanosheet systems, which was attributed to the π–π restacking of the nanosheets. This strongly corroborates with the findings of Jiang and co-workers[79] that the arms of TPE can be effectively locked in the COF structure. In this case, however, the restricted planarization of TPE locked it in a conformation that prohibits enhanced fluorescence.

3.3.2. Pyrene-containing COFs. In 2008, Jiang and co-workers synthesized a fluorescent, pyrene-containing COF *via* co-condensation between pyrene diboronic acid (PDBA) and hexahydroxytriphenylene (HHTP) vertex units to form TP-COF.[81] The incorporation of HHTP units into the structure allowed for a wide absorbance range, from ultraviolet to visible regions, however the emission band remained narrow due to a favorable singlet energy transfer process between excited HHTP and nearby pyrene units. Shortly after, in 2009, Jiang and co-workers also synthesized a boroxine-linked COF *via* self-condensation of PDBA to form the strongly fluorescent PPy-COF.[82] The dramatic 63 nm redshift of PPy-COF's emission compared to PDBA was attributed to excimer formation due to close face-to-face stacking of pyrene units (Fig. 10).

In 2016, a variety of imine-linked, pyrene-containing COFs were synthesized by condensing 1,3,6,8-tetrakis(4-amino-phenyl)pyrene with a variety of linear dialdehydes.[83] The synchronization effect of the twisted phenyl substituents led to a highly crystalline COF whose intra- and interlayer electronics could be tuned based on the dialdehyde linkers employed. Despite exhibiting poor photoluminescence quantum yields (Φ_{PL} < 1%), it was revealed that the COF systems were capable
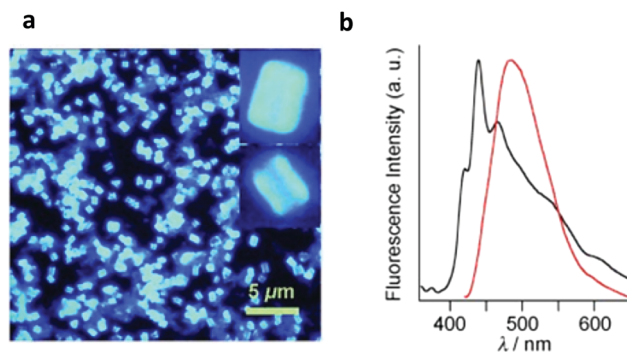

Fig. 10 (a) Fluorescence microscopic image of PPy-COF (the inset depicts an enlarged image of individual cubes). (b) Normalized fluorescence spectra (λ_{ex} = 414 nm, 25 °C) of PDBA (black curve) and PPy-COF (red curve). Adapted with permission from *Angew. Chem., Int. Ed.*, 2009, **48**, 5439–5442.

of delocalizing excitations along the pyrene stacks and that interlayer charge-transfer excitations *via* the imine bonds were taking place.

In 2016, three dehydrobenzoannulene (DBA)-containing COF systems were synthesized by McGrier and co-workers *via* co-condensation between PDBA and either DBA[12], DBA[18], or a 1:1 ratio of each to give Py-DBA-COF 1, Py-DBA-COF 2, or Py-MV-DBA-COF, respectively (Fig. 11).[84] All three systems showed strong fluorescence due to AIE from the DBA monomers. The fluorescence emission for Py-DBA-COF 2 (λ_{em} = 483 nm) was notably higher in energy than that of Py-DBA-COF 1 (λ_{em} = 530 nm). This was attributed to the symmetry-forbidden nature of excitations for the DBA[12] vertex in Py-DBA-COF 1. Interestingly, the mixed vertex variant, Py-MV-DBA-COF, also exhibited a redshifted (λ_{em} = 528 nm) emission spectrum, indicating that DBA[12] primarily dominated its excited-state properties (Fig. 12).

In 2018, Lotsch and co-workers[85] synthesized three azine-linked COFs by condensing hydrazine with 1,3,6,8-tetrakis-(4-ethynylbenzaldehyde)-pyrene (TEBPY), 1,3,6,8-tetrakis(6-ethynylnicotinaldehyde)-pyrene (TENPY), and 1,3,6,8-tetrakis-(2-ethynylpyrimidin-5-carb-aldehyde)pyrene (TEPPY) to form A-TEBPY-COF, A-TENPY-COF, and A-TEPPY-COF, respectively (Fig. 13). According to DFT calculations, the addition of alkynes between the porphyrin and phenyl units allowed for improved planarization of the overall monomers. As a result, all three COF systems exhibited a reduced interlayer stacking distance (3.43 Å) compared to previously reported, less planar systems (3.9–4.33 Å).[86,87] The increased planarity also led to the formation of both in-plane extended conjugation and out-of-plane excimers, which allowed the system to emit a broad low energy emission band (λ_{em} = 670–700 nm).

3.3.3. Hydrogen bond-containing COFs. Fluorescent COFs containing boroxine or boronate ester linkages tend to be highly emissive. The chemical instability of these linkages has since led to the incorporation of nitrogen-centered linkages. Unfortunately, the use of these linkages often sacrifices photoluminescence for enhanced stability. These diminished photoluminescence quantum yields have been attributed to the imine
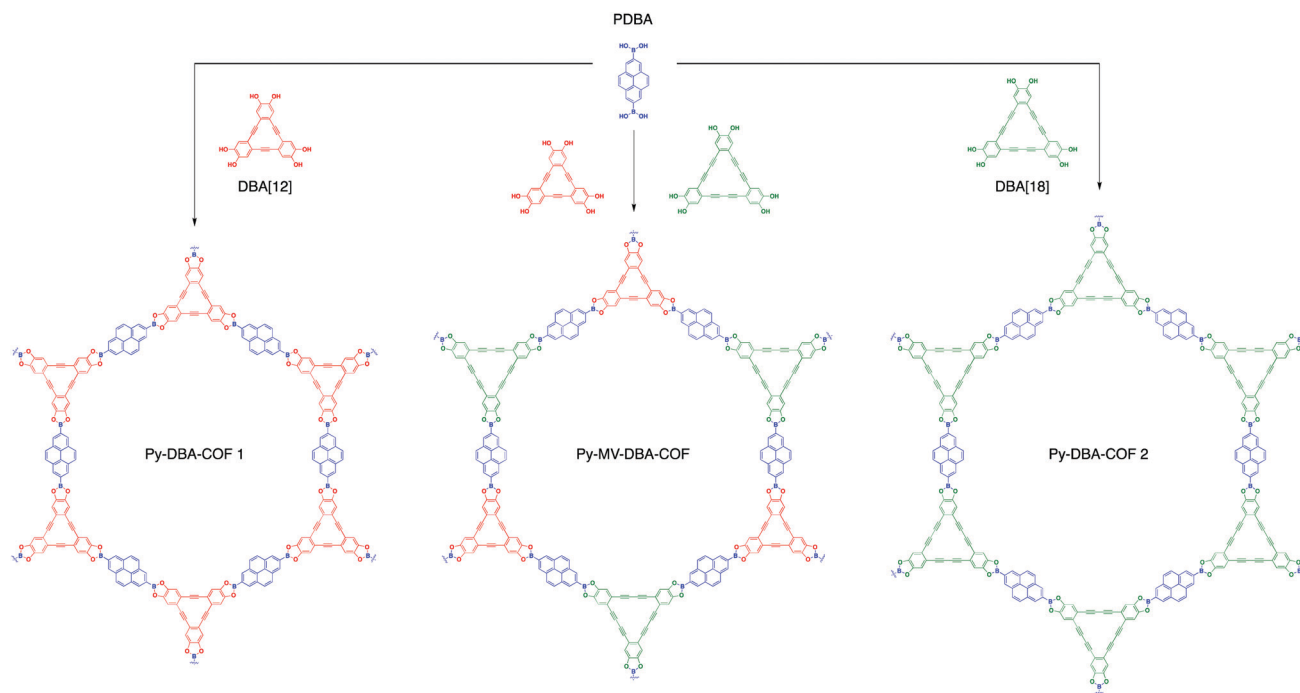
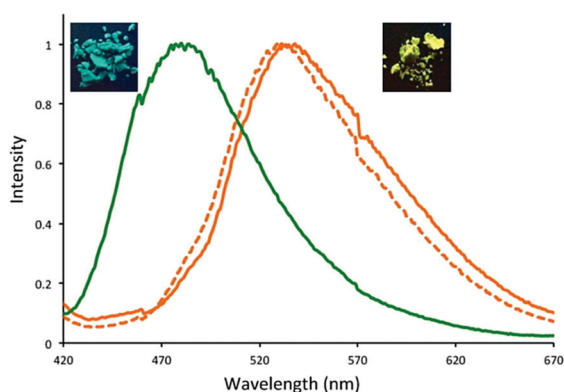Fig. 11 Synthesis of Py-DBA-COF 1, Py-MV-DBA-COF, and Py-DBA-COF 2.

Fig. 12 Normalized emission spectra of Py-DBA-COF 1 (orange, λ_{ex} = 350 nm), Py-DBA-COF 2 (green, λ_{ex} = 365 nm), and Py-MV-DBA-COF (dashed orange, λ_{ex} = 350 nm). Photographs of the fluorescent solids were taken using a hand-held UV-lamp at 365 nm. Reprinted with permission from *J. Am. Chem. Soc.* 2016, **138**, 10120−10123. Copyright 2016 American Chemical Society.

X, Y = CH: TEBPY
X = N, Y = CH: TENPY
X, Y = N: TEPPY

Fig. 13 The acetic acid catalyzed condensation of hydrazine and pyrene-based aldehyde linkers to form various azine-linked COFs.

4. Exploiting the photophysical properties of COFs for practical applications

4.1. Chemical sensing

One application that luminescent COFs are particularly suited for is chemical sensing. The porous nature of COFs allows potential analytes to diffuse through the pore channels. This property not only allows for molecular recognition, but also the potential removal of analytes. Furthermore, the modular nature of COFs allows for the design of polymeric materials that are useful for chemical sensing. Explosives and metal cations have both been popular analytes in the field of COF-based chemical sensing. Several groups have also investigated the detection of other analytes such as ammonia, chiral molecules, and hydroxyl radicals.

linkage's ability to non-radiatively decay through rotational and vibrational relaxation pathways.[88] Loh and co-workers utilized the planarizing effects of hydrogen bonding in order to enhance the fluorescence of systems linked through atoms other than boron, while also greatly expanding the scope of AIE-active systems (Fig. 14).[89] By using hydrozone linkages with neighboring hydroxyl/ether-containing substituents, multiple hydrogen-bonding sites could be incorporated into the system. The intra- and interlayer hydrogen bonds effectively inhibited the rotational relaxation pathway, allowing for strong (Φ_f = 16.3%) fluorescence in the solid state. Additionally, a dual emission could be produced in the solid state by simply incorporating an allylic ether.
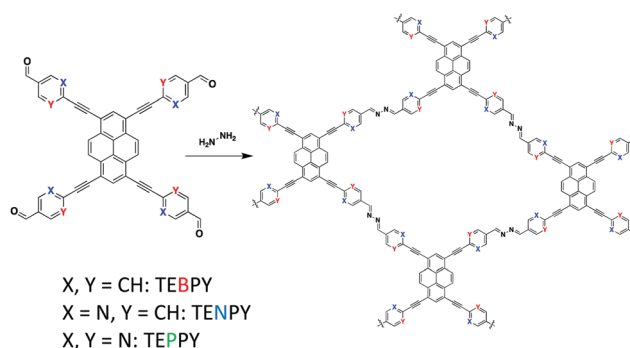
848 | *Chem. Soc. Rev.*, 2020, **49**, 839−864

This journal is © The Royal Society of Chemistry 2020

a

Free intramolecular bond rotation

b

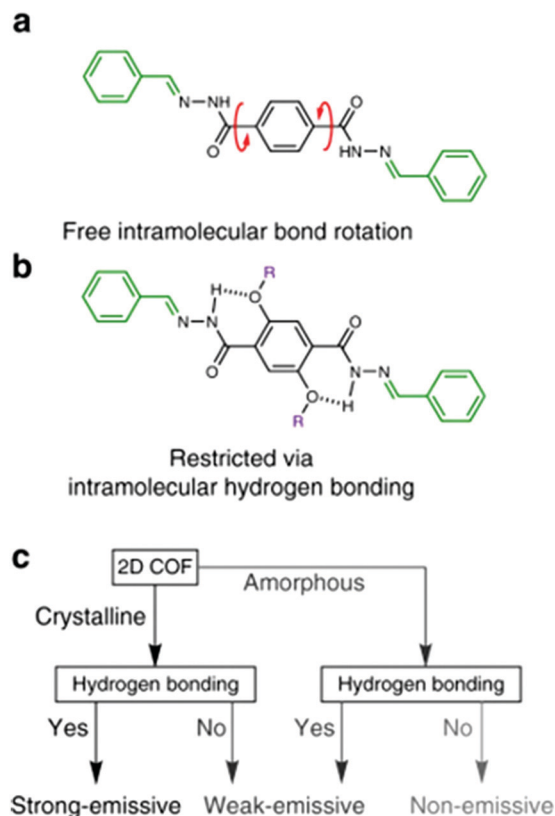Restricted via
intramolecular hydrogen bonding

c

Fig. 14 (a) Free intramolecular rotation in the amorphous solid state makes it non-emissive. (b) Intramolecular hydrogen bonding restricts rotation, causing enhanced emission in the UV to violet region. (c) Flow chart depicting the strategy to achieve strong solid state emission in 2D COFs. Adapted with permission from *Nat. Commun.*, 2018, **9**, 233.

4.1.1. Explosives. Jiang and co-workers investigated COFs as chemosensors in 2013 when they utilized their azine-linked COF (Py-azine COF) in the detection of 2,4,6-trinitrophenol (TNP).[86] Py-azine COF stacked in an AA eclipsed arrangement which created a fluorescent channel to serve as a chemosensing detector. It was revealed that the azine units on the edges acted as open docking sites and could form hydrogen-bonding interactions with guest molecules. This hydrogen-bonding interaction is believed to be the main contributor to inducing fluorescence quenching of the material. A variety of nitroaromatic compounds were tested along with TNP including 2,4-dinitrophenol (DNP), 2,4-dinitrotoluene (DNT), 2-nitrophenol (NP), and 2-nitrotoluene (NT). The fluorescence was quickly quenched in the presence of TNP vapor. The fluorescence was quenched up to 69% when the concentration of TNP was as low as 70 parts per million (ppm). The other compounds did not have any significant effect on the fluorescence of the material (Fig. 15). Time-resolved fluorescence spectroscopy was utilized to investigate the quenching mechanism. The lifetime of Py-azine COF remained the same with different concentrations of TNP, consistent with a static fluorescence quenching mechanism. The studies indicated that Py-azine COF could be a promising candidate for selective TNP detection.

In 2018, Zhao and co-workers developed two imine-linked, heteroporous, fluorescent COFs that exhibited fluorescence
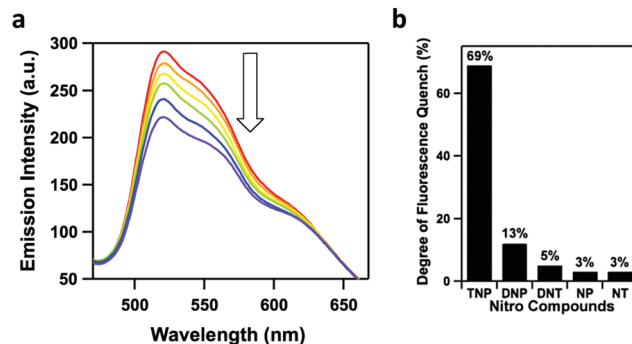

Fig. 15 (a) Fluorescence quenching of Py-azine COF in MeCN (0.01 mg mL^{-1}) upon exposure to TNP vapors for various times (0–70 min). (b) Degree of fluorescence quenching after the addition of various nitro compounds (70 ppm). Adapted with permission from *J. Am. Chem. Soc.* 2013, **135**, 17310–17313. Copyright 2013 American Chemical Society.

quenching in the presence of small quantities of TNP.[90] The two COFs were designed by the condensation of a C_{2v} symmetric building block with a linear linker yielding COF-BABD-BD and COF-BABD-BZ. Powder X-ray diffraction (PXRD) and pore size distribution analysis was employed to confirm the AB stacking pattern of the 2D COF layers. It was hypothesized that the slip-stacked arrangement may have reduced any potential aggregate caused quenching (ACQ). During the sensing experiments, a nitroaromatic compound (TNP, DNP, DNT, 1,3-dinitrobenzene, *p*-nitrotoluene, or nitrobenzene) was slowly introduced into a suspension of the COF in acetonitrile. TNP induced significant fluorescence quenching of each COF while other nitroaromatic compounds had no significant effect on the fluorescence of the COFs (Fig. 16a–c) indicating that they may be used as effective chemical sensors for the presence of TNP with good selectivity and sensitivity. The acetonitrile suspensions changed color upon the introduction of TNP from golden yellow to dark brown indicating the material could be used as visual chemosensors with the naked eye (Fig. 16d). Stern–Volmer quenching constants (K_{SV}) were calculated to quantify the sensitivity of the COFs towards different nitroaromatic compounds resulting in K_{SV} values of 5.7×10^5 M^{-1} and 4.5×10^5 M^{-1} for COF-BABD-BD and COF-BABD-BZ, respectively, for TNP. These constants are ten to one hundred times larger than for the other tested nitroaromatic compounds and support the observation that the COFs are highly selective towards TNP sensing.

A photoluminescent TPE-based imine-linked COF was reported by the Loh and co-workers in 2018.[91] This COF was also utilized to sense TNP. 1,3,6,8-Tetrakis(4-aminophenyl)-pyrene and 1,1,2,2-tetrakis(4-formylphenyl)ethane were chosen as the building blocks due to their fluorescent and AIE properties yielding Py-TPE-COF. Transmission electron microscopy (TEM) images showed that Py-TPE-COF crystallized as sphere-like nanoparticles with domain sizes of 300–500 nm. The nanoparticles displayed solvatochromism when dispersed in THF, acetone, acetonitrile, or DMF, emitting either a bright blue or blue-green luminescence with PL bands centered at 462, 469, 474, and 493 nm, respectively (Fig. 17). The fluorescence
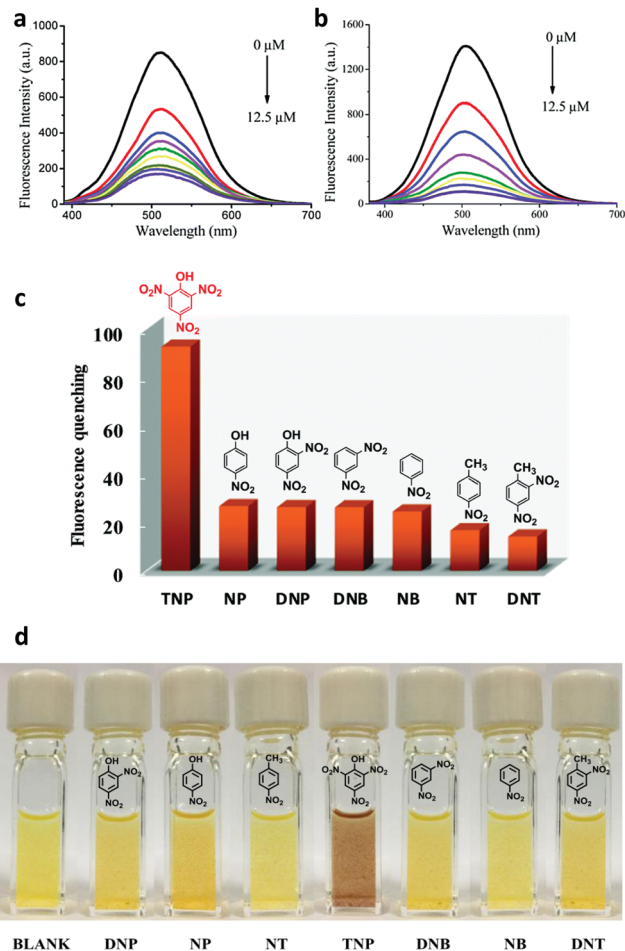
This journal is © The Royal Society of Chemistry 2020

Chem. Soc. Rev., 2020, **49**, 839–864 | 849

Fig. 18 (a) Photograph of 3D-Py-COF powder under UV light irradiation. (b) Fluorescence quenching of 3D-Py-COF in DMF upon addition of TNP (0–20 ppm). Reprinted with permission from *J. Am. Chem. Soc.*, 2016, **138**, 3302–3305. Copyright 2016 American Chemical Society.

Fig. 16 Fluorescence spectra (λ_{ex} = 370 nm) of (a) COF-BABD-DB and (b) COF-BABD-BZ dispersed in MeCN with the addition of varying amounts of TNP. (c) Fluorescence quenching (%) of COF-BABD-BZ with different nitroaromatics (12.5 μM). (d) Photographs of COF-BABD-DB dispersed in MeCN with the addition of various nitroaromatics (4.0 μM). Adapted from *Chem. Commun.*, 2018, **54**, 2308–2311, with permission from the Royal Society of Chemistry.
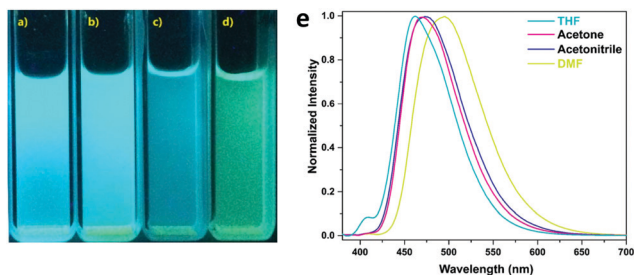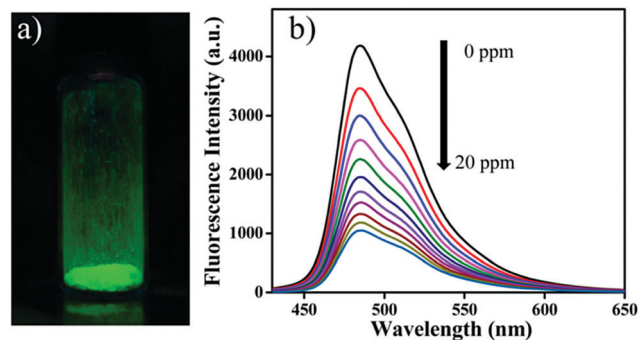
Fig. 17 Photographs of Py-TPE COF dispersed in (a) THF, (b) acetone, (c) acetonitrile, and (d) DMF, while illuminated by UV-light (365 nm). (e) Normalized fluorescence spectra (λ_{ex} = 365 nm) of Py-TPE-COF dispersed in different solvents. Adapted from *Chem. Commun.*, 2018, **54**, 2349–2352, with permission from the Royal Society of Chemistry.

was attributed to the use of the nonplanar TPE groups that should reduce π–π interactions, prevent ACQ, and thus enhance PL. Furthermore, as spherical COF nanoparticles, a curvature-induced

strain was introduced, that may have acted to prevent any rotations in the imine linkages. Fluorescence quenching experiments with TNP were performed in acetone. An addition of 1 ppm of TNP solution caused a sharp decrease in fluorescence of the COF nanoparticles. Several other nitroaromatic compounds were tested to investigate the selectivity of the fluorescence quenching towards TNP including DNP, DNT, NT, and NP. Only small decreases in PL were measured indicating Py-TPE-COF could be used as a chemical sensor selective for TNP detection. It was suggested that the fluorescence quenching may result from the hydroxy group on TNP hydrogen-bonding with a nitrogen on the pore walls of the COF. This non-emissive complex could then trap the excitation energy, resulting in static fluorescence quenching.

Wang and co-workers used a luminescent 3D COF (3D-Py-COF) for explosives detection (Fig. 18).[92] Tetra(*p*-amino-phenyl)methane and 1,3,6,8-tetrakis(4-formylphenyl) pyrene were chosen as the tetrahedral (3D-T_d) and rectangular (2D-C_2) building blocks, respectively. Their condensation yielded an imine-linked 3D-COF with a *pts* topology that displayed a yellow-green luminescence. TNP was employed to investigate the chemical sensing properties of the 3D COF. TNP was gradually added to a suspension of 3D-Py-COF in DMF. The COF exhibited 75% fluorescence quenching after the addition of 20 ppm of TNP with a quenching constant (K_{SV}) of $3.1 \times 10^4 \text{ M}^{-1}$. The fluorescence quenching is most likely due to an electron transfer process. The energy levels of the HOMOs and LUMOs of 3D-Py-COF and TNP were investigated using the DFTB-D method. Results indicated that the electron transfer from the HOMO of 3D-Py-COF to the LUMO of TNP is facilitated upon photoexcitation.

4.1.2. Metal cations. An early application of a fluorescent COF for the detection of metal cations was reported in 2016 by Wang and co-workers.[93] They synthesized a fluorescent thioether-functionalized hydrazine-linked COF, COF-LZU8, to sense and remove Hg^{2+} (Fig. 19a). COF-LZU8 showed strong fluorescence in both the solid state and when dispersed in solvent. This fluorescence, which was not exhibited by the monomers, was attributed to the extended conjugation of the material and possibly to contributions by the thioethers. It was
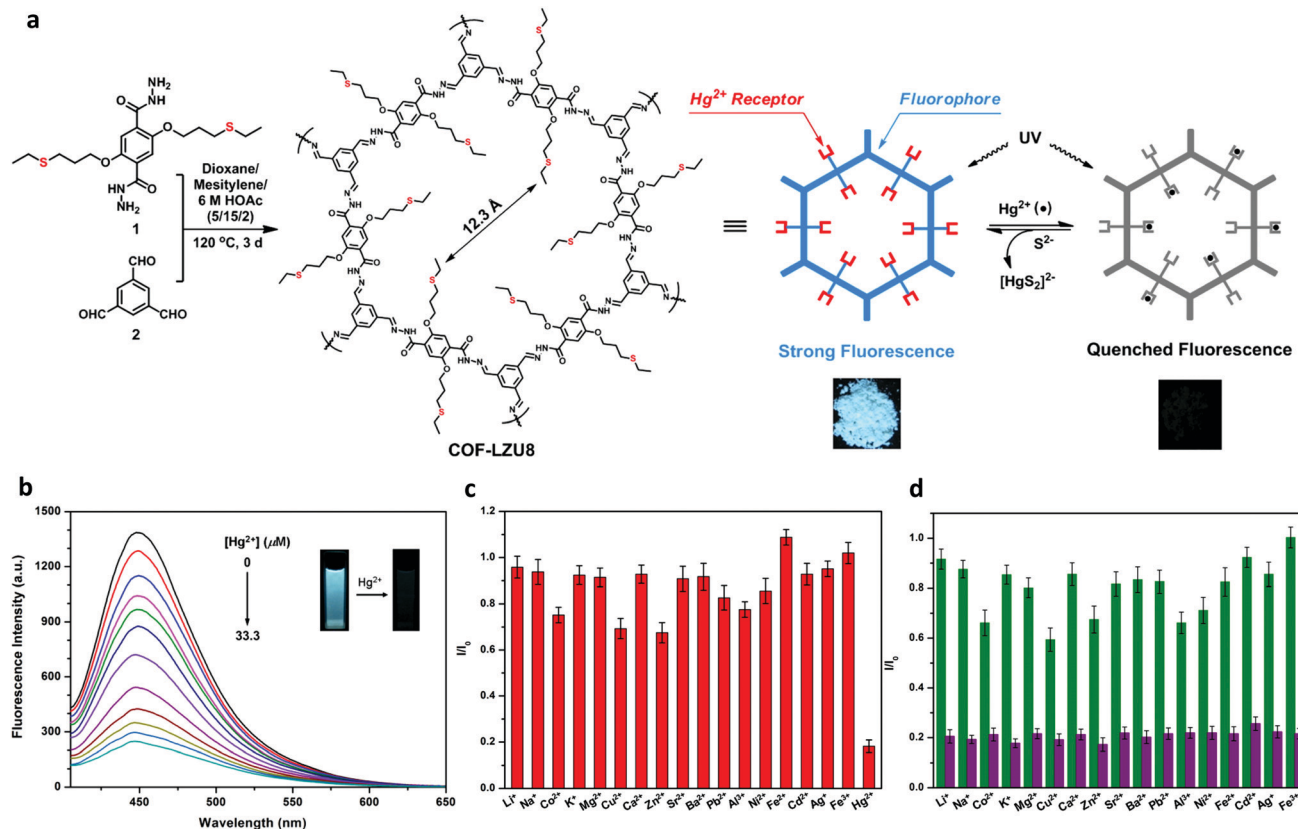
850 | *Chem. Soc. Rev.*, 2020, **49**, 839–864

This journal is © The Royal Society of Chemistry 2020

Fig. 19 (a) Synthesis of COF-LZU8 and the proposed mechanism for fluorescence quenching by Hg^{2+} (photographs taken of COF-LZU8 under UV lamp, 365 nm). (b) Fluorescence quenching of COF-LZU8 dispersed in MeCN upon the addition of Hg^{2+} (λ_{ex} = 390 nm). (c) Fluorescence of COF-LZU8 with different metal ions in MeCN (λ_{ex} = 390 nm). (d) Competition experiment of the emission intensity of COF-LZU8 in the presence of competitive ions (2.0 equiv., green bars) and the resulting intensity upon the addition of Hg^{2+} (1.0 equiv., purple bars). Adapted with permission from *J. Am. Chem. Soc.*, 2016, **138**, 3031–3037. Copyright 2016 American Chemical Society.

noted that the contorted structure of the material's 2D layers may prevent any potential ACQ. The incorporation of thioether sidechains allowed COF-LZU8 to act as an ionophore for the detection of Hg^{2+}. The effective sensing of Hg^{2+} was noticeable to the naked eye, as the material showed efficient fluorescence quenching upon the addition of Hg^{2+} under a UV lamp (Fig. 19b). The quenching is thought to arise from Hg^{2+} binding to sulfur atoms resulting in a transfer of electrons from the π-conjugated framework to the unoccupied Hg^{2+} orbitals. The selectivity and sensitivity of this system was further investigated by examining the quenching response in the presence of competitive cations. The detection limit for Hg^{2+} was determined to be 25 parts per billion (ppb). The selectivity was investigated by testing several other metal cations (Li^+, Na^+, Co^{3+}, K^+, Mg^{2+}, Cu^{2+}, Ca^{2+}, Zn^{2+}, Sr^{2+}, Ba^{2+}, Pb^{2+}, Al^{3+}, Ni^{2+}, Fe^{2+}, Cd^{2+}, Ag^+, and Fe^{3+}) (Fig. 19c and d). Of these metal cations, only Hg^{2+} showed significant fluorescence quenching. The selectivity is thought to arise from the strong interactions between Hg^{2+} and the sulfur atoms in COF-LZU8, as evidenced by X-ray photoelectron spectroscopy (XPS) and solid-state NMR. A reduction in the concentration of Hg^{2+} in water was also noted indicating the successful removal of Hg^{2+} by COF-LZU8. Recycling studies showed that the COF could go through the

adsorption–desorption process at least three times without significant loss of activity.

Liu and co-workers constructed a hydrogen bond assisted azine-linked COF (COF-JLU3) for the sensing of Cu^{2+} cations.[37] 1,3,5-tris(3′-*tert*-butyl-4′-hydroxy-5′-formylphenyl)benzene and hydrazine hydrate were used as the building blocks. The inclusion of –OH groups on the trialdehyde monomer allowed for an intramolecular hydrogen-bonding interaction with a nitrogen from the nearby azine linkage, which imparted enhanced crystallinity and chemical stability (Fig. 20a). The *tert*-butyl groups were shown to impact the π–π interactions between the 2D layers, effectively enhancing the luminescence of the material. The redshift in the absorption band of COF-JLU3 in comparison to the monomers indicated the role of extended conjugation in the material's fluorescent properties. These structural characteristics were possibly responsible for the sensing of Cu^{2+}. For the sensing experiments, the COF was dispersed in THF before the introduction of $M(NO_3)_x$ with a variety of metal ions (Li^+, Na^+, K^+, Mg^{2+}, Ca^{2+}, Ba^{2+}, Zn^{2+}, Cd^{2+}, Ni^{2+}, Pb^{2+}, Co^{2+}, Cu^{2+}, Ag^+, Fe^{3+}, Al^{3+}) at 2×10^{-1} mol L^{-1}. It was observed that alkaline, alkaline-earth, and transition metal ions with filled d shells had little effect on the luminescence intensity of the COF. Metal ions with different electronic
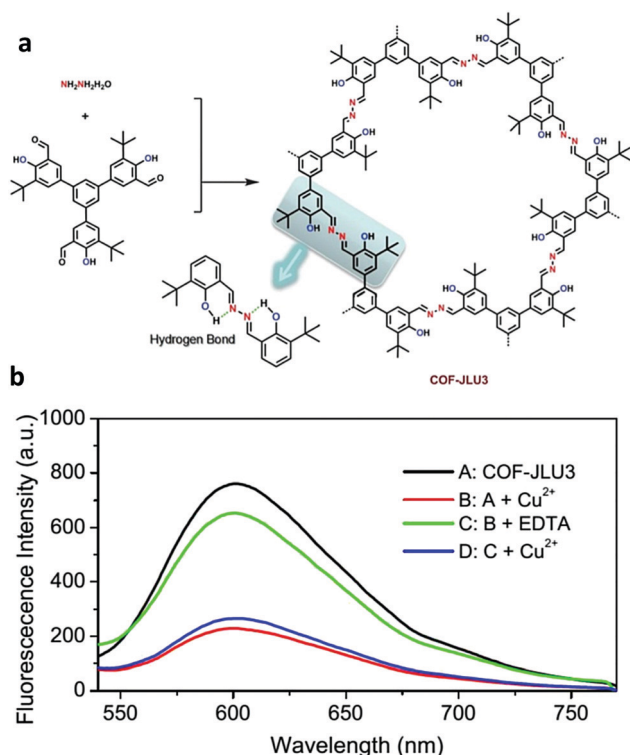
This journal is © The Royal Society of Chemistry 2020

Chem. Soc. Rev., 2020, **49**, 839–864 | 851

Fig. 20 (a) Synthesis of COF-JLU3 depicting the intramolecular hydrogen bonding. (b) Fluorescence spectra of COF-JLU3 demonstrating its effective reversible quenching by Cu^{2+} ions. Adapted from *Chem. Commun.*, 2016, **52**, 6613, with permission from the Royal Society of Chemistry.

configurations such as Fe^{3+}, Cu^{2+}, and Co^{2+} exhibited a larger influence on luminescence of the COF. Cu^{2+} caused the largest change. After the addition of two equivalents of the Cu^{2+} ion, COF-JLU3 retained only 18.3% of its original luminescence intensity. XPS measurements indicated Cu^{2+} ions were successfully immobilized in the COF pore which contained multiple binding sites such as the hydroxyl groups and nitrogen atoms on the pore wall. The binding of the metal leads to the fluorescence quenching of the system *via* a photoinduced electron transfer (PET) process. Interference studies were employed with competing cations and different counterions were also investigated. Ultimately, it was determined that the addition of other cations and the nature of the anion had no significant effect on the luminescence of COF-JLU3. Recyclability studies showed that fluorescence could be regained after the removal of Cu^{2+} ions and quench again upon reintroduction (Fig. 20b).

A series of four 2D imine-linked COFs were investigated for their Fe^{3+} sensing abilities by Yan and co-workers.[94] 1,3,5-Tri-(4-aminophenyl) benzene (TaPb), terephthaldehyde (TpTa), 1,3,5-tri-(4-aminophenyl) triazine (Tz) and 2,5-dihydroxy-terephthaldehyde (Da) were employed as the building blocks to obtain the four COFs (TaTa, DhaTab, TRITER-1 and TzDa). Multiple metal cations were utilized to probe the possibility of metal ion detection (Na^+, Mg^{2+}, K^+, Ca^{2+}, Cu^{2+}, Zn^{2+}, Pb^{2+}, Ag^+, Al^{3+}, Fe^{3+}, and Cd^{2+}). Of these only Fe^{3+} showed a significant effect on the fluorescence quenching of each COF. The K_{SV}

values for COFs TaTa, DhaTab, TRITER-1 and TzDa were determined to be 1.4×10^4, 1.0×10^5, 5.6×10^3, and 3.3×10^3 M^{-1}, respectively. It was suggested that this fluorescence quenching was caused by absorption competition quenching. In contrast to the other metal cations tested, Fe^{3+} had a UV-vis absorption from 250–400 nm. This absorption overlapped with those of the COFs. The order of increasing overlap was DhaTab > TaTa > TRITER-1 > TzDa, which matched the pattern of the quenching constants indicating this could very likely have been the source of fluorescence quenching.

Zhang and co-workers sought to develop a COF that could detect Fe^{3+} by exploiting the fact that Fe^{3+} will chelate to the O,N,O′ moiety of salicylaldehyde benzoyl hydrazone (SBH) to form a strong coordination complex (Fig. 21).[95] O,N,O′-Chelating units were introduced into a COF structure by employing benzene-1,3,5-tricarbohydrazide (Bth) with 2,5-dihydroxytere-phthalaldehyde (Dha) or 2,5-dimethoxyterephthalaldehyde as building units yielding COFs Bth-Dha and Bth-Dma, respectively. Bth-Dma displayed a strong fluorescence, attributed to restricted bond rotation, therefore, this COF was utilized in Fe^{3+} detection experiments. The metal sensing experiments were carried out by introduction of chloride salts at 100 μM to Bth-Dma suspensions. The addition of Na^+, K^+, Mg^{2+}, Ba^{2+}, Mn^{2+}, Ca^{2+}, Gd^{3+}, or Al^{3+} to the COF suspension led to almost no change in luminescence intensity while the addition of Zn^{2+}, Ni^{2+}, Co^{2+}, La^{3+}, Nd^{3+}, Fe^{2+}, or Cu^{2+} led to a marginal decrease in luminescence. However, the introduction of Fe^{3+} led to a significant quenching of luminescence. A K_{SV} of 2.3×10^4 M^{-1} was obtained from Stern–Volmer plots with a detection limit of 0.17 μM. Changes in pH and anion had no effect on the fluorescence quenching indicating Bth-Dma is selective towards Fe^{3+}. The fluorescence quenching was thought to arise from energy or electron transfer that occurs after the O,N,O′-Fe^{3+} coordination with excited states involving d-orbital electrons. This binding event was supported by XPS measurements after soaking Bth-Dma in $FeCl_3$ for two days.

4.1.3. Ammonia. In 2016, Jiang and co-workers published their work on the development of a fluorescent boronate ester linked COF (TPE-Ph COF) that employed a TPE building block.[79] TPE-Ph COF was investigated for the chemical sensing of ammonia. The Lewis acidic boron in the boronate ester linkage in the COF was capable of forming a Lewis acid–base pairing with the Lewis basic nitrogen in ammonia. TPE-Ph COF exhibited a decrease in luminescence upon the addition of ammonia (Fig. 22). A rate constant of 6.3×10^{14} M^{-1} s^{-1} for 1 ppm of ammonia and 0.25 mg of COF in 2 mL of toluene was measured. This high fluorescence quenching rate constant indicated that TPE-Ph COF could be a good candidate for a sensitive ammonia sensor at sub ppm levels.

4.1.4. Chiral species. Two fluorescent chiral COFs (CCOFs) were utilized by Cui and co-workers to sense the chirality of a class of terpene flavor molecules.[96] 1,1′-Bi-2-naphthol (BINOL) can act as both a source of chirality and fluorescence. Therefore, the BINOL-based ligand 6,6′-dichloro-2,2′-diethoxy-1,1′-binaphthyl-4,4′-dialdehyde (BINOL-DA) was utilized. It was paired with tetrakis(4-aminophenyl)ethene or 1,3,5-

852 | *Chem. Soc. Rev.*, 2020, **49**, 839–864

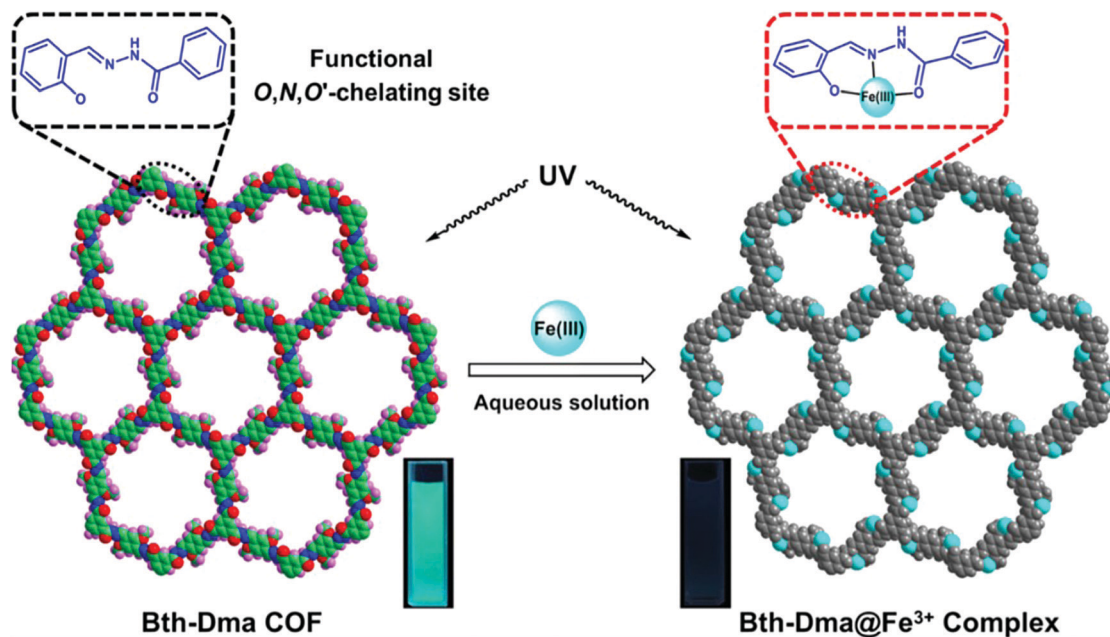This journal is © The Royal Society of Chemistry 2020

Fig. 21 Structure of Bth-Dma COF with and without the addition of Fe^{3+}. Inset photographs show the fluorescence quenching upon the formation of Bth-Dma@Fe^{3+} complex. Reprinted with permission from *ACS Appl. Mater. Interfaces*, 2019, **11**, 12830–12837. Copyright 2019 American Chemical Society.
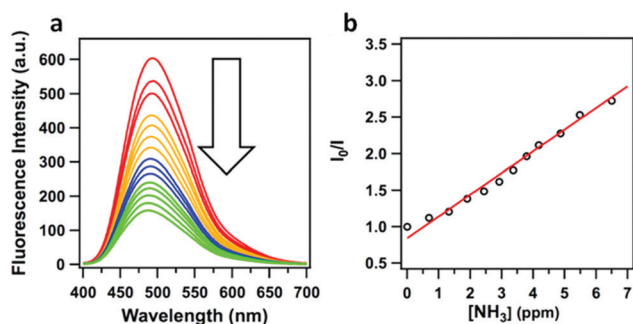

Fig. 22 (a) Fluorescence quenching of TPE-Ph COF upon the addition of ammonia. (b) Stern–Volmer plot of the ammonia driven fluorescence quenching of TPE-Ph COF. Adapted with permission from *J. Am. Chem. Soc.*, 2016, **138**, 5797–5800. Copyright 2016 American Chemical Society.

tris(4-amino-3,5-diisopropylphenyl)benzene yielding CCOFs 7 and 8, respectively. Initial sensing experiments were carried out after synthesizing CCOF 7 with enantiopure (*R*)-BINOL-DA. Fluorescent CCOF 7 was exfoliated into nanosheets (NS) *via* solvent-assisted liquid sonication. The fluorescence of the 7-NS was blueshifted in comparison to the bulk powder, likely a result of the decreased π–π interactions. Different amounts of (−)- and (+)-enantiomers of the substrates were added to a suspension of 7-NS in acetonitrile (Fig. 23). The addition of (α)-pinene caused a decrease in fluorescence emission, but the rate of quenching differed. The (−)-enantiomer quenched at a faster rate with a calculated quenching ratio of 3.41. The opposite stereoselectivity was observed when employing (*S*)-7-NS. 7-NS also exhibited enantioselectivity towards limonene, fenchone, terpinen-4-ol, and carvone. Electrospinning was employed
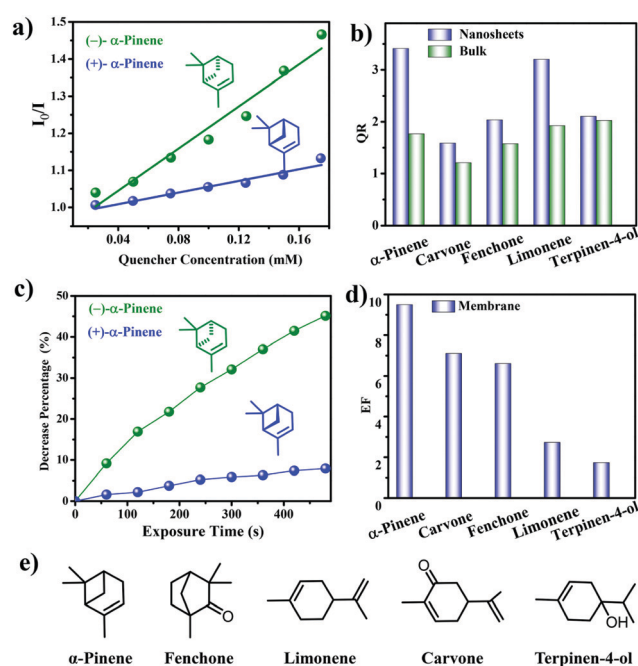

Fig. 23 (a) Stern–Volmer plots of 7-NS in MeCN after titration of α-pinene. (b) Enantioselective quenching ratios for various terpenes. (c) Decreased fluorescence (%) of 7@PVDF upon introduction of α-pinene. (d) Enantioselective quenching ratios for various terpene vapors. (e) Structures of terpenes used. Reprinted with permission from *J. Am. Chem. Soc.*, 2019, **141**, 7081–7089. Copyright 2019 American Chemical Society.

to immobilize 7-NS as free-standing nanofiber membranes (7@PVDF) as may be done in a practical application. The enantioselective fluorescence decrease ratio of (α)-pinene was
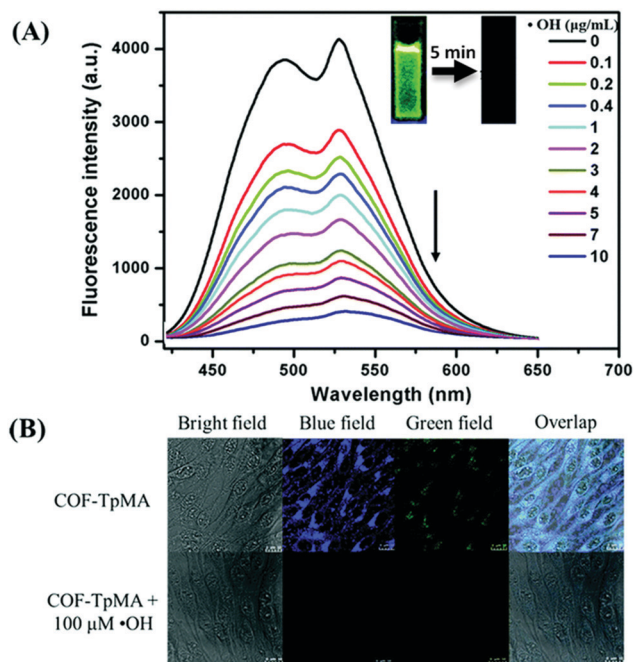
This journal is © The Royal Society of Chemistry 2020

Chem. Soc. Rev., 2020, **49**, 839–864 | 853

Fig. 24 (A) Fluorescence quenching of COF-TpMA upon the addition of •OH. (B) Confocal laser scanning microscopy images of BHK cells treated with COF-TpMA (top) and pretreated with COF-TpMA and then treated with •OH (bottom). Scale bar = 10 μm. Reproduced from *Chem. Commun.*, 2019, **55**, 167–170, with permission from the Royal Society of Chemistry.

calculated to be 9.5. This membrane also showed enantio-selectivity towards other chiral vapors including limonene, fench-one, terpinen-4-ol, and carvone. Ultimately, after exfoliating CCOF 7 into nanosheets, it could be used to detect chiral odor vapors in both the solution and membrane form. Consistent fluorescent lifetimes for both 7-NS and 7@PVDF were measured before and after addition of (−)-α-pinene indicating the static nature of the complexation.

4.1.5. Hydroxyl radicals. COF-TpMA was synthesized *via* the mechanochemical grinding of triformylphloroglucinol (Tp) and melamine (MA).[97] The resulting luminescent COF was then utilized for the detection of hydroxyl radicals (•OH) (Fig. 24A). The fluorescence of the COF was ascribed to extended conjugation and limited intramolecular bond rotation. COF-TpMA displayed weak absorption at 283 nm. This absorption strength increased upon the introduction of •OH and the color changes from colorless to brown. The absorbance intensity increased linearly with •OH concentration. However, the fluorescence intensity centered at 530 nm decreased in intensity with the addition of •OH. Other reactive oxygen species tested did not exhibit any effect on the fluorescence of COF-TpMA. The fluorescence quenching was attributed to the electron transfer of hydroxyl radicals to the framework. Fluorescent lifetimes are consistent with a static fluorescence quenching mechanism. The COF was tested to have low cytotoxicity below 60 μg mL^{-1}. Cells were then incubated with COF-TpMA before the introduction of •OH into the cells. Fluorescence quenching could be observed during this process (Fig. 24B). This demonstrates that

COFs can be applied towards bioimaging and the detection of •OH in living cells.

4.2. Photocatalysis

The utilization of COFs as photocatalysts has seen significant interest. The insolubility and stability of COF frameworks allows for the facile use as heterogeneous catalysts, while the modular nature of their design allows for the precise integration of functional building units. Due to the large number of works in this area, this section will highlight recent progress in a few of the investigated transformations.

4.2.1. *E–Z* isomerization. Banerjee and co-workers used TpTt to photocatalyze the uphill conversion of *trans*-stilbene to *cis*-stilbene using visible light (blue LEDs).[38] The triazine core of TpTt promotes the transformation *via* strong π–π interactions with the *E*-alkenes, while the keto functionalities in the β-ketoenamine core help enhance the lifetime of the excited triplet state. Calculations indicate that the mechanism goes through (1) TpTt absorbs visible light and goes from $S_0 \rightarrow S_1$, (2) ISC to reach the more energetically stable T_1 state, and finally (3) interaction with the *trans*-stilbene wherein the photoexcited TpTt transfers its energy to the stilbene, providing the energy for the isomerization (Fig. 25).

4.2.2. Hydrogen evolution. Lotsch and co-workers utilized a COF for photocatalytic hydrogen evolution using visible light.[98] Combination of 2,5-diethoxy-terephthalohydrazide (DETH) and 1,3,5-tris-(4-formyl-phenyl)triazine (TFPT) yielded hydrazone-linked TFPT-COF. The UV/vis spectrum of the yellow TFPT-COF showed an absorption edge around 400 nm, corresponding to an optical band gap of ∼2.8 eV. This band gap is within the required range for water splitting and hydrogen evolution (1.9–3.1 eV).[99] Incorporation of Pt as the photon reduction catalyst (PRC) and sodium ascorbate as the sacrificial electron donor into the photosensitizer TFPT-COF allowed for successful catalytic hydrogen evolution. In fact, the TFPT-COF/Pt produced 230 μmol h^{-1} g^{-1}. When 10 vol% aqueous triethanolamine (TEOA) was used as the sacrificial donor, an enhanced hydrogen evolution rate of 1970 μmol h^{-1} g^{-1} was observed, corresponding to a quantum efficiency of 2.2%. TEM and PXRD of the used photocatalyst showed a loss of long-range order as the material exfoliated in water. It was determined that despite the loss of long-range order, the material did not decompose. Additionally, the amorphous product was easily able to regain its crystalline structure through treatment with the initial synthesis conditions. Despite exfoliating in the aqueous solution, the TFPT-COF/Pt system continually produced hydrogen for up to 24 h.

In 2018, Bein and co-workers reported the utilization of a COF as a photocathode for light-driven water electrolysis.[59] The synthesized BDT–ETTA COF combined the geometric, crystalline, and interlayer stacking influences of 1,1′,2,2′-tetra-*p*-amino-phenylethylene (ETTA)[100] with benzo[1,2-*b*:4,5-*b′*]dithiophene-2,6-dicaroxaldehyde (BDT), a donor-type dithiophene. When grown as thin films, the combination of nearly planar p-type functional monomers with polarizable imine linkages resulted in a conjugated BDT–ETTA film capable of acting as a
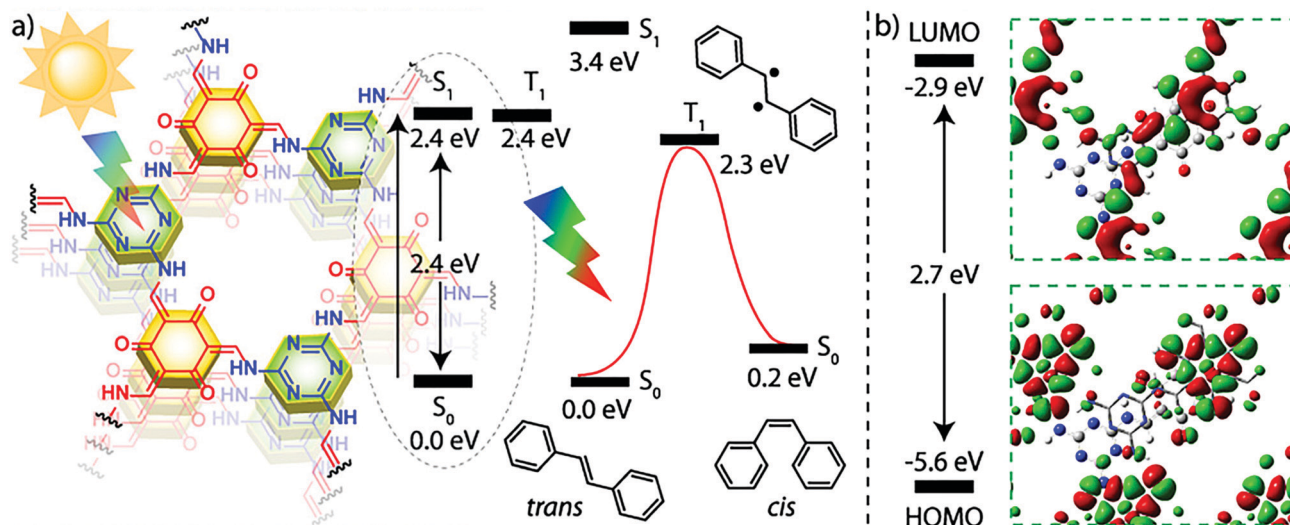
854 | *Chem. Soc. Rev.*, 2020, **49**, 839–864

This journal is © The Royal Society of Chemistry 2020

Fig. 25 (a) Representation of the proposed mechanism for the TpTt COF photocatalyzed *E–Z* isomerization of stilbene. (b) Graphic representation of the HOMO and LUMO orbitals of TpTt and their energy levels (the orbital energy levels are not to scale). Reprinted with permission from *J. Am. Chem. Soc.*, 2019, **141**, 6152–6156. Copyright 2019 American Chemical Society.

photocathode to facilitate photoelectrochemical water splitting without the use of a sacrificial agent or a co-catalyst. The BDT–ETTA films showed strong absorbance of visible light, with a direct optical band gap (2.47 eV), HOMO (−5.51 eV), and LUMO (−3.34 eV) that are favorable for photoelectrochemical water splitting. The photoexcited electrons on the COF film's surface were capable of spontaneously transferring to the electrolyte, due to the LUMO being higher in energy than the H_2O/H_2 redox pair, resulting in water splitting. As intended, the photoactivity of the system came from the BDT building units, while the high orientation of the COF films not only improved stability, but also amplified the photoresponsiveness of the system.

Lotsch and co-workers utilized a series of triphenylaryl-aldehydes, with varying concentrations of nitrogens (N_x) in the central aryl ring, to tune a 2D-COF for photocatalytic water reduction (Fig. 26).[101] The hydrogen evolution activity increased with the nitrogen content of the monomers, reaching a maximum of 1703 μmol h^{-1} g^{-1} for N_3-COF (Fig. 26c). This trend was attributed to a combination of several factors including increasing planarity to facilitate exciton migration within the COF plane, the electronic character of the central aryl ring, the ability of the sacrificial electron donor to efficiently remove the hole from the photoexcited COF, and the relative stabilities of the radical formed in the catalytic process. Despite the complexity of the effects that the structural changes had on the photocatlytic activity of the COFs, this work demonstrates the significant impact that structural and electronic properties have on the photocatalytic properties of the resulting COFs.

4.2.3. C–C bond forming reactions. The direct derivatization of quinoxalin-2(1*H*)-ones has significant impact on the drug discovery process.[102] Yang and co-workers[103] were able to use the photoactivity of hydrazide-linked 2D-COF-1 for the visible-light driven C3 arylation and alkylation of quinoxalin-2(1*H*)-ones (Fig. 27). With the use of K_2CO_3 as a base, DMSO as the solvent,

and various hydrazines as the aryl and alkyl sources, 2D-COF-1 under blue LED irradiation was capable of the C3 derivatization with a broad functional group tolerance. It was proposed that the reaction proceeds through an initial photoexcitation of 2D-COF-1 which subsequently reduces molecular oxygen to generate an oxygen radical and superoxide radical anion. The activated oxygen then oxidizes the hydrazine to produce the nucleophilic carbon radical which attacks the electron deficient quinoxalin-2(1*H*)-one. The produced radical intermediate then proceeds through a single electron transfer (SET) with 2D-COF-1$^+$ to turn over the photocatalyst.

The alteration of electron donor–acceptor pairs in polymeric structures is known to strengthen charge carrier transport mobility. Thomas and co-workers[104] utilized this principle in the design of two thiophene-based 2D-COFs (TTT-DTDA and TTT-BTDA). Both COFs proved to be effective radical initiators for visible light driven free radical polymerization (Fig. 28). Irradiation of the COF samples led to charge separation as seen by electron paramagnetic resonance (EPR). When combined with triethylamine (TEA) as a co-initiator, the system promoted the radical polymerization of methyl methacrylate (MMA) to form poly-methyl methacrylate (PMMA) with conversions as high as 63% after 12 h for TTT-DTDA, compared to ~54% for TTT-BTDA under the same conditions. The heightened yield for TTT-DTDA could be attributed to better charge transfer separation as *in situ* EPR analysis showed a slower rate for undesired electron–hole pair recombination events, while also showing a more pronounced radical formation in the photocatalyst.

4.2.4. Photoreductive dehalogenation. Liu and co-workers used the photoelectric activity of pyrene units to assemble a donor–acceptor type 2D-COF (COF-JLU22).[105] COF-JLU22 displayed broad electronic adsorption (λ_{max} = 510 nm), ranging from the visible to near IR region, and had an optical band gap
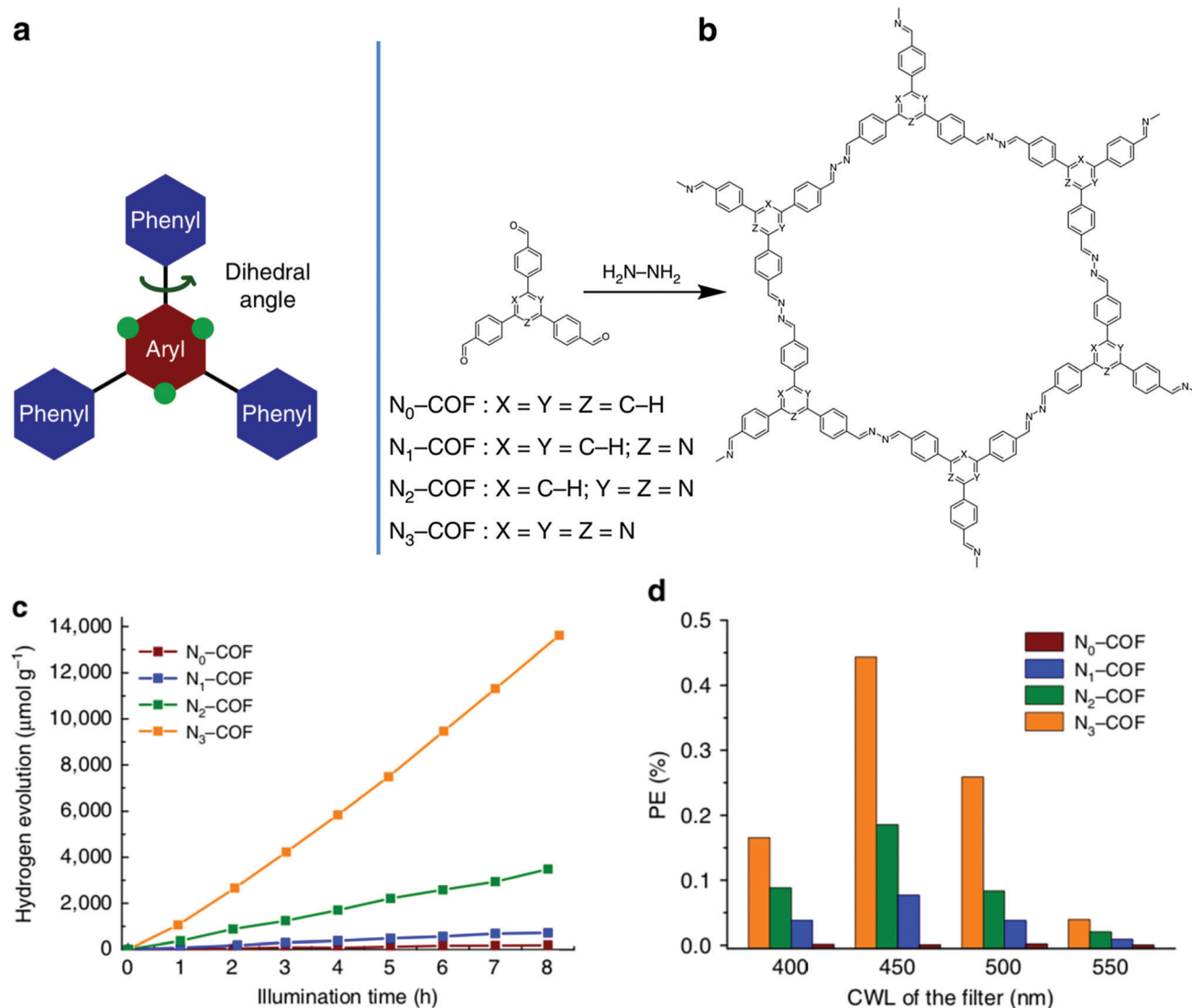
Fig. 26 (a) Depiction of the tunable nature of the triphenylarene platform. Swapping 'C–H' groups to nitrogen atoms at the green dots effects the planarity of the aryl monomer. (b) Synthesis of N_x-COFs from hydrazine and N_x-Ald monomers. (c) Hydrogen evolution by N_x-COF photocatalysts over 8 h, using triethanolamine as the sacrificial electron donor. (d) The photonic efficiency (PE) of N_x-COFs using different band-pass filters with central wavelengths (CWLs) at 400, 450, 500, and 550 nm. Adapted with permission from *Nat. Commun.*, 2015, **6**, 8508.

of 2.08 eV. The photoexcitable COF-JLU22 was implemented for the photoreductive dehalogenation of phenacyl bromide derivatives under visible-light irradiation (30 W green LED, 520 nm). The mechanism (Fig. 29) is believed to go through an initial photoexcitation of the COF to generate holes and electrons through charge separation. The excited electron is then transferred from the conduction band (CB) of the COF ($E_{1/2}$ = −0.86 V) to the phenacyl bromide ($E_{1/2}$ = −0.49 V) causing homolytic cleavage of the C–Br bond. The use of Hantzsch ester allows for a hydrogen atom source that can be abstracted by the generated α-carbonyl radical. Meanwhile the photogenerated hole in COF-JLU22 extracts an electron from the sacrificial *N,N*-diisopropylethylamine (DIPEA), returning COF-JLU22 to its ground state. In addition, COF-JLU22 was shown to be an effective catalyst for the photoinduced α-alkylation of aldehydes using alkyl bromides.

4.2.5. Degradation of organic contaminants. Giesy and co-workers were able to utilize the highly stable and porous TpMA COF as a radical initiator for the photo-degradation of organic contaminants (Fig. 30).[106] TpMA was capable of complete degradation of phenol after 60 min of irradiation with visible light, compared to removal efficiencies below 12% without the use of light. The total organic carbon of the solution after irradiation was measured and indicated that up to 45.6% of the phenol was mineralized. Additionally, the catalytic photo-degradation of methyl orange by TpMA was demonstrated to proceed with 89% degradation after 60 min of irradiation. The TpMA COFs were proposed to catalyze the photo-degradation by initial activation of molecular oxygen *via* electron transfer from the photoexcited TpMA.

Jiang and co-workers were able to substantially enhance the catalytic activity of a porphyrin-based COF through the
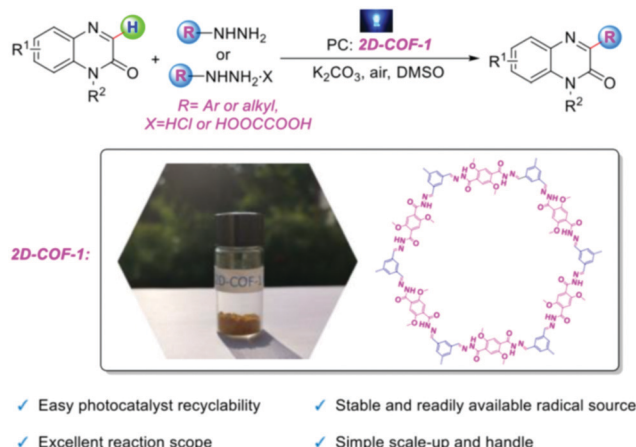
856 | *Chem. Soc. Rev.*, 2020, **49**, 839–864

This journal is © The Royal Society of Chemistry 2020

Fig. 27 The use of 2D-COF 1 as a photocatalyst for the direct C3 arylation and alkylation of quinoxalin-2(1*H*)-ones. Adapted with permission from *Chem. – Eur. J.*, 2020, **26**, 369–373.
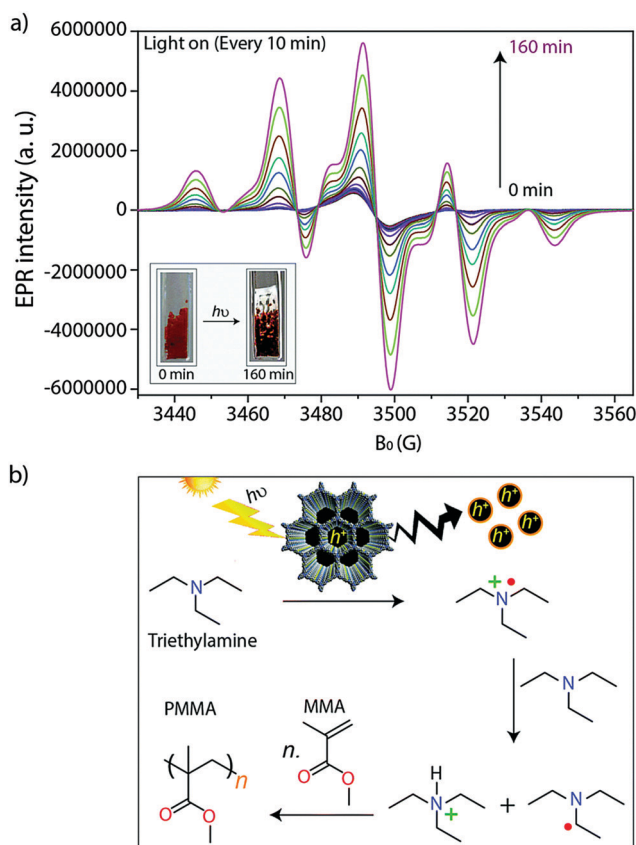

Fig. 28 (a) *In situ* EPR spectra during the photocatalyzed free radical polymerization of MMA to PMMA. (b) Proposed mechanism for the TTT-DTDA (or TTT-BDTA) catalyzed conversion of MMA to PMMA. Reproduced from *Chem. Sci.*, 2019, **10**, 8316–8322, with permission from the Royal Society of Chemistry.

incorporation of graphitic carbon nitride (g-C$_3$N$_4$) to form CuPor-Ph-COF/g-C$_3$N$_4$ hybrid composites.[107] The heterojunction-containing composites significantly outperformed both the pure g-C$_3$N$_4$ and CuPor-Ph-COF for the photo-degradation of
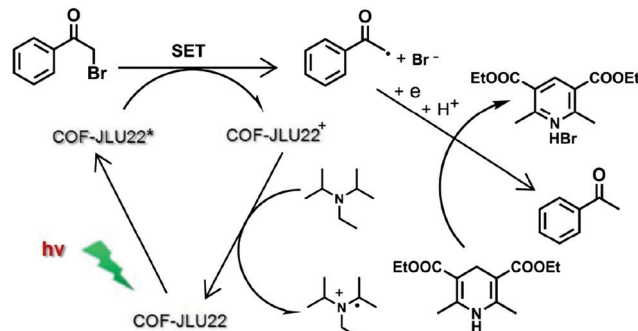

Fig. 29 Proposed mechanistic representation of the COF-JLU22 catalyzed photoreductive dehalogenation. Adapted with permission from *Appl. Catal., B*, 2019, **245**, 334–342.
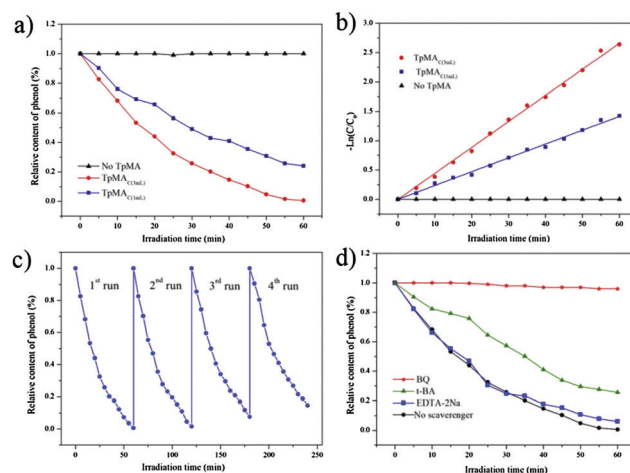

Fig. 30 (a) Visible light irradiated photocatalytic degradation of phenol. (b) Linear simulation $-\ln(C/C_0) = kt$ of the kinetic curves. (c) Recyclability of TpMA. (d) Scavenger effects on the photo-degradation of phenol. Reprinted with permission from *J. Hazard. Mater.*, 2019, **369**, 494–502.

rhodamine B (RhB), a common organic pollutant, showing removals of 86, 36, and 23%, after 90 min of visible-light irradiation, respectively. This increased activity was attributed to an increased visible light absorption and faster charge carrier transfer within the hybrid material. XPS and UV-vis spectra showed that CuPor-Ph-COF had a valence band (VB) and CB that were 0.79 eV and 0.61 eV lower in energy than g-C$_3$N$_4$, respectively. These results suggested that the photo-excited electrons on the CuPor-Ph-COF migrate to the g-C$_3$N$_4$ through the interface. Simultaneously, the holes generated on the g-C$_3$N$_4$ transfer to the CuPor-Ph-COF, resulting in efficient charge separation and increased photocatalytic activity (Fig. 31).

4.3. White-light emitters

In addition to chemical sensors and photocatalysts, COFs are of significant interest for solid-state luminescent devices. This is particularly the case for white-light emitters, due to the ability to control the photophysical properties with molecular
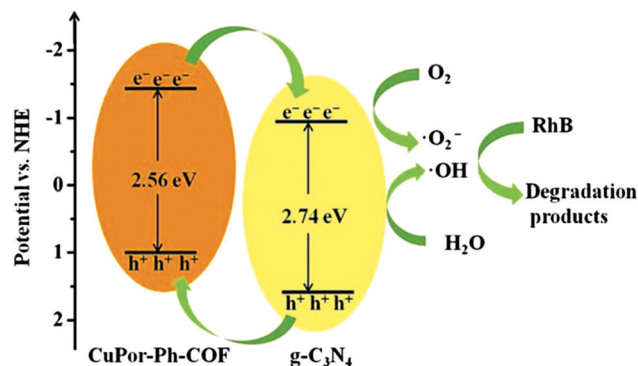
Fig. 31 Proposed mechanism for the photocatalytic degradation of rhodamine B by CuPor-Ph-COF/g-C₃N₄ hybrid composite. Reproduced from *Dalton Trans.*, 2019, **48**, 14989–14995, with permission from the Royal Society of Chemistry.

precision. Loh and co-workers demonstrated this level of tunability by synthesizing hydrogen-bonding COF systems using a variety of linkers (Fig. 32).[89] Due to the increased conjugation, the systems with longer linkers showed a red-shifted emission. In addition, dual emissions were observed for some systems depending on the extent of inter- and intralayer

hydrogen bonding. The highest absolute photoluminescence quantum yield observed for the 9 reported systems was 16.3%. It was found that a dual emission (Φ_{PL} = 7.3%) could also be induced by incorporating allyl groups into a multi-component system and that, by doing so, CIE coordinates of (0.30, 0.38) were obtained. These coordinates closely approach those of pure white light (0.33, 0.33).

Another method for obtaining white-light emission is by simultaneously emitting blue, red, and green light from one source. Van der Voort and co-workers utilized this *via* co-condensation of 4,4′,4″-(1,3,5-triazine-2,4,6-triyl)trianiline (TTA) and 2,6-diformylpyridine (DFP) to form TTA-DFP-COF as a blue-emitting, imine-linked COF.[108] The material was subsequently grafted with Eu^{3+} and Tb^{3+} ions chelated with β-diketonate ligands (Fig. 33).[108] Due to the particular chelation environment around the lanthanide ions, excitation of 10%Eu90%Tb@TTA-DFP-COF (Φ_f = 3.1%) and 1%Eu99%Tb@ TTA-DFP-COF (Φ_f = 2.8%) gave calculated CIE coordinates of (0.3636, 0.3355) and (0.3442, 0.3801), respectively.

Solvatochromism can be utilized to induce white-light emission. Vaidhyanathan and co-workers achieved this by incorporating 2,4-dihydroxybenzene-1,3,5-tricarbaldehyde and anthracene-2,6-diamine to form IISERP-COF7 (Fig. 34a).[77] When dispersed
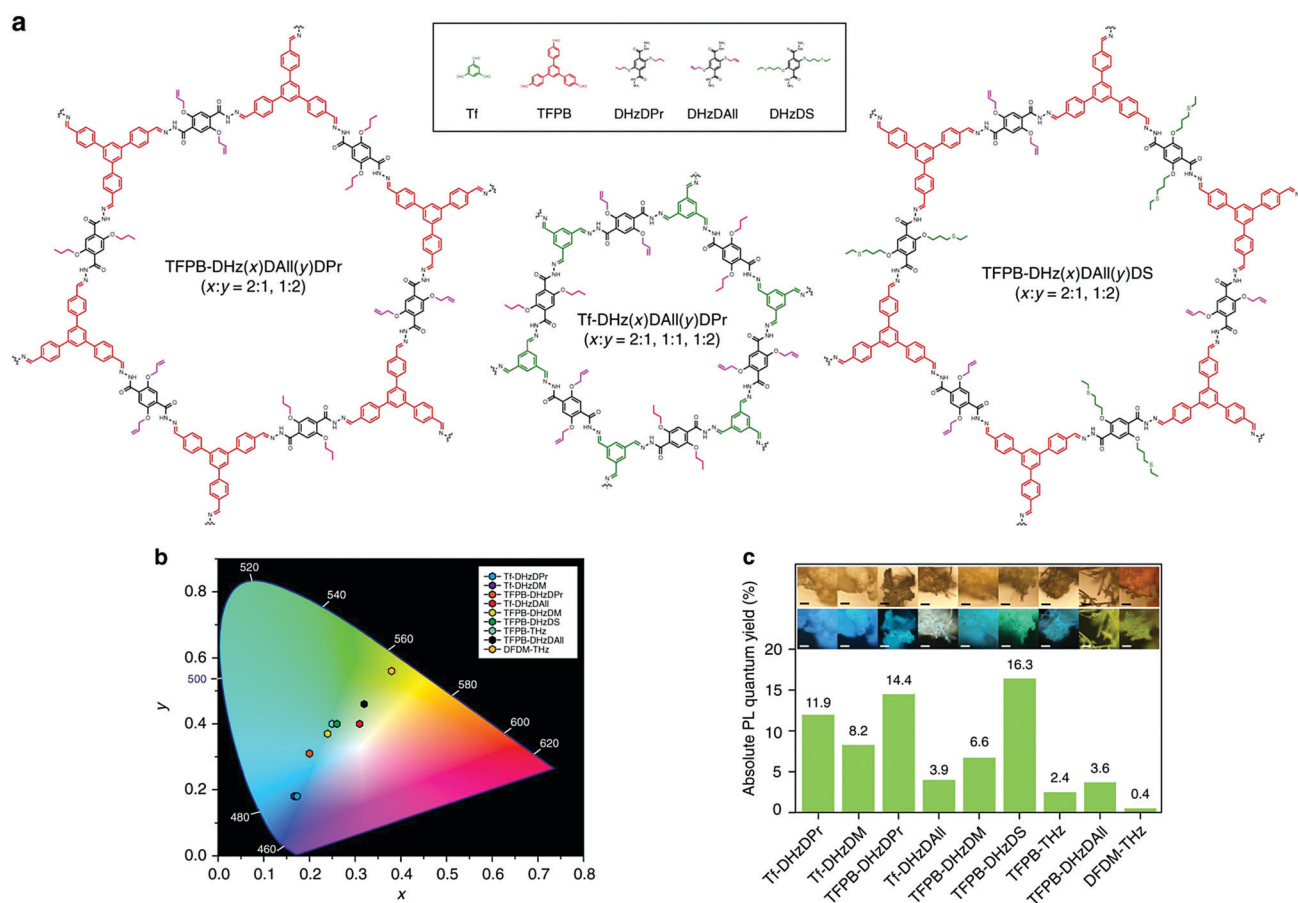
Fig. 32 (a) Synthetic scheme for obtaining the series of multicomponent COFs for the fine-tuning of PL emission. (b) CIE diagram of various COFs. (c) Absolute PL quantum yields for various COFs; inset depicts fluorescence microscopic images of COFs under visible (top) and UV (bottom) light (scale bar = 50 μm). Adapted with permission from *Nat. Commun.*, 2018, **9**, 2335.

858 | *Chem. Soc. Rev.*, 2020, **49**, 839–864

This journal is © The Royal Society of Chemistry 2020

Fig. 33 Synthetic scheme for the formation of TTA-DFP COF and the subsequent grafting of lanthanides. Reprinted with permission from *ACS Appl. Mater. Interfaces*, 2019, **11**, 27343–27352. Copyright 2019 American Chemical Society.

in various common solvents, IISERP-COF7 displayed a wide range of emission wavelengths. It was determined through UV-vis experiments that the anthracene units provided a blue fluorescence. The hydroxyl functionalities yielded a dual emission as a result of enol and β-ketoenamine taut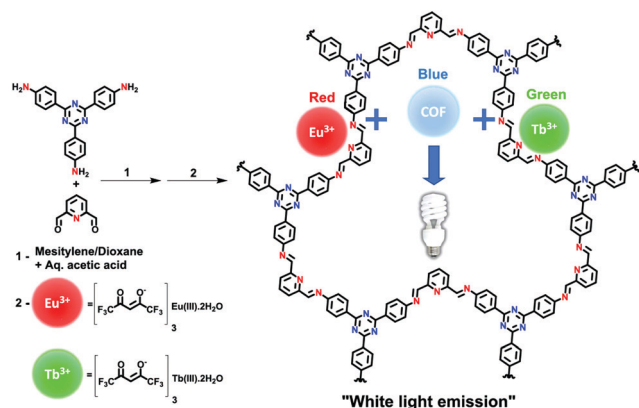omers. The tautomerization equilibrium was strongly affected by the base or hydrogen-bonding capability of the solvent, as discussed in a previous section, which influenced the overall emission energy.

When dispersed in NMP, a white-light emission was observed due to NMP's ability to satisfy a 50:50 ratio of tautomers. In addition, NMP improved the fluorescence lifetime via transition state stabilization. Flexible thin films could be fabricated (COF@PMMA) using 0.32 wt% COF, providing a single-source white-light emitter with CIE coordinates of (0.35, 0.36) which could be adjusted to (0.29, 0.33) simply by reducing the amount of COF present in the film to 0.30% (Fig. 34b and c).

Recently, Weng and co-workers successfully fabricated a COF-coated LED for white-light emission.[39] By co-condensing TPE with the tetrahedral-shaped tetrakis-(4-aminophenyl)-methane (TAPM), 3D-TPE-COF was constructed and exhibited a two-fold interpenetrated structure with a bright yellow emission (Φ_{PL} = 20%) was constructed. 3D-TPE-COF was then mixed with an epoxy resin to act as a coating for a blue LED (Fig. 35), which yielded calculated CIE coordinates of (0.30, 0.35). Interestingly, the stability of the system persisted over 1200 h of continuous emission at ambient conditions.

4.4. Photodetectors

In 2017, Bein and co-workers[109] sought to develop a COF that possessed absorption capabilities in the near-infrared (NIR) spectral regions to employ in the fabrication of a COF-based NIR photodetector. This was accomplished by combining electron-rich and -deficient moieties in the same building block to hopefully allow charge-transfer transitions to take place at
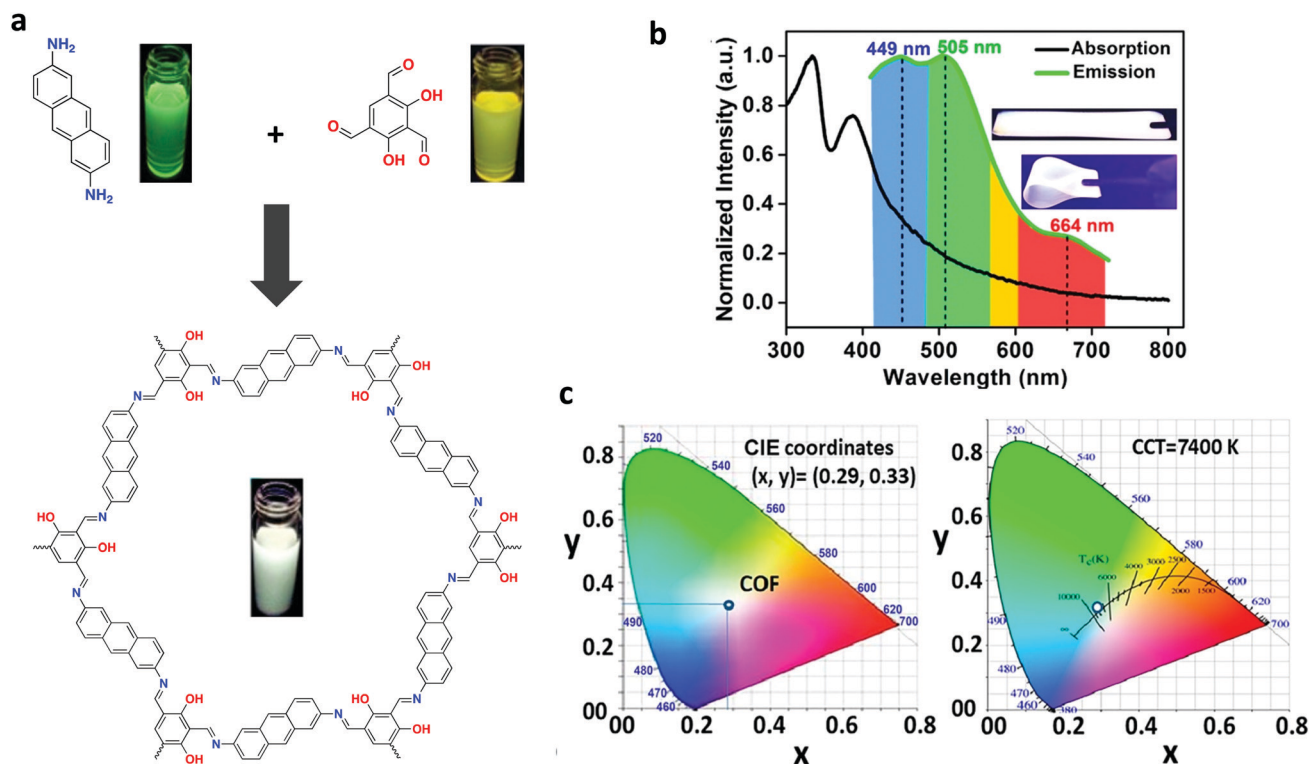

Fig. 34 (a) Synthesis of IISERP-COF7, including photographs of monomers and COF dispersed in NMP under a UV lamp. (b) Solid state absorption and emission spectra of COF@PMMA (λ_{ex} = 420 nm), with inset photographs of COF@PMMA film under UV irradiation. (c) CIE coordinate and CCT diagram of COF film with a thickness of 2 mm. Adapted with permission from *J. Am. Chem. Soc.*, 2018, **140**, 13367–13374. Copyright 2018 American Chemical Society.
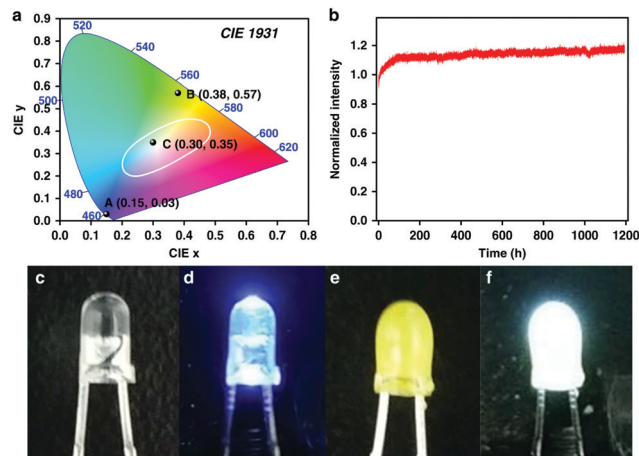
Fig. 35 (a) CIE diagram of blue LED (A), 3D-TPE-COF (B), and COF-coated LED (C). (b) Normalized emission intensity for the COF-coated LED over 1200 h, at 2 mA. Photographs of reference blue LED when off (c) and on (d), COF-coated LED when off (e) and on (f). Reprinted with permission from *Nat. Commun.*, 2018, **9**, 5234.

energies below the π–π* transition. A material absorbing in the NIR spectral region should enhance its light harvesting capabilities in photovoltaic devices. Isoindigo and thieneoisoindigo-based building blocks were utilized to construct a series of 2D imine-linked COFs. Ultimately, 5,5′-bis(2-formylthiophen5-yl)-*N*,*N*′-dibutyl-thienoisoindigo (tTII) was paired with 1,3,6,8-tetrakis(4-aminophenyl)pyrene (Py) yielding Py-tTII COF, which was utilized in thin film growth. The UV-vis spectra showed strong absorption bands in the blue and red-NIR regions. Py-tTII COF was grown on MoO_x-modified indium-tin oxide transparent electrodes with [6,6]-phenyl C_{71} butyric acid methyl ester ($PC_{71}BM$) to form an interdigitated heterojunction as part of a COF-based NIR photodetector. The device, COF:$PC_{71}BM$, exhibited an absorbance from 300 to 1100 nm. This work revealed that it is possible to switch the spectral response from blue- and red-sensitive to green- and NIR-sensitive by changing the bias voltage made possible by the growth of the thin COF film.

4.5. Thermometers

Van Der Voort and co-workers demonstrated the use of COFs as luminescent ratiometric thermometers *via* a lanthanide grafting process. 1,3,5-Triformylphloroglucinol (Tp) and 2,2′-bipyridine-5,5′-diamine (Bpy) were first combined to form TpBpy, which produced a broad emission band between 400–550 nm at room temperature.[110] The material was soaked in solutions containing excess amounts of lanthanide ions complexed with acetylacetone, which was chosen as a ligand due to its high-lying triplet level, thus making it energetically compatible with the lanthanide ions used. The resulting lanthanide-grafted COFs, TpBpy-Ln_acac (Ln = Eu^{3+}, Tb^{3+}, Eu^{3+}/Tb^{3+}, Dy^{3+}), were able to function as solid-state thermometers in the 10–360 K range for Eu/Tb systems, as well as the 280–440 K temperature ranges for Dy systems (Fig. 36). Interestingly, in Eu/Tb systems, there was a noted lack of thermal quenching. This phenomenon was attributed to the absence of ion-to-ligand/host
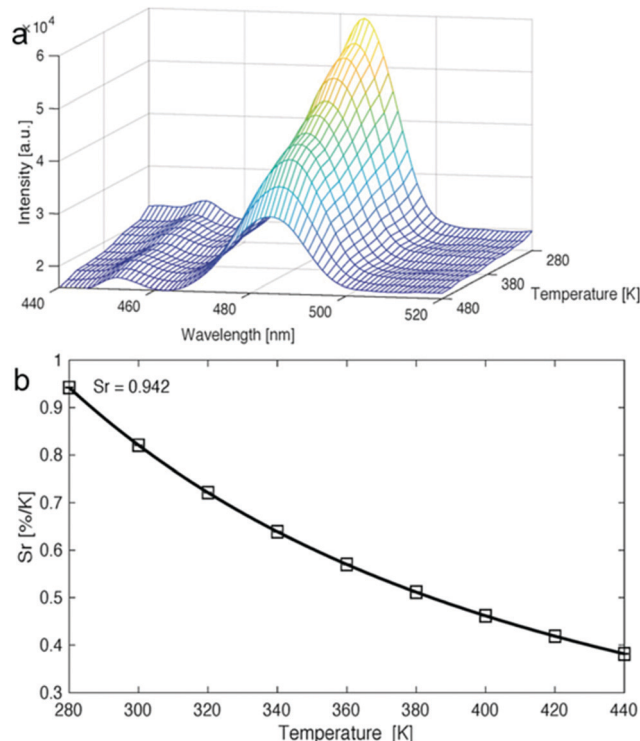

Fig. 36 (a) Emission map of Dy(acac)$_3$-grafted TpBpy COF material recorded at 280–480 K. (b) Represenation of the relative sensitivity values for the same compound at varying temperatures. Reprinted with permission from *Angew. Chem., Int. Ed.*, 2020, **59**, 2–11.

energy transfer. It was also determined that no Tb^{3+}-to-Eu^{3+} energy transfer was occurring within the material, which was attributed to large spatial separation between ions within TpBpy. For a summary of COFs discussed in the application section see Table 1.

5. Conclusions

In summary, the modular nature of COFs permits the integration of various π-conjugated monomers to construct 2D and 3D polymeric materials with unique photophysical properties. However, the conditions necessary for obtaining good quantum yields are highly linkage-dependent, and it is now understood that fluorescent imine-linked COFs are particularly challenging due to the rotational and vibrational relaxation pathways that lead to non-radiative decay. By reinforcing the planarity of the imine bond, incorporating highly fluorescent subunits like anthracene, or utilizing AIE phenomena with monomers such as TPE, the radiative decay pathways can be reprogrammed to overcome the non-radiative decay processes. Extended conjugation through C=C linkages is also successful in producing fluorescent systems, and further extension with longer linkers can be a useful method to tune the photophysical properties of the overall system. Bulk COF powders dispersed in various solvents are also capable of exhibiting solvatochromism.

With the development of novel methodologies came a diverse set of processing alternatives that allowed for applications

860 | *Chem. Soc. Rev.*, 2020, **49**, 839–864

This journal is © The Royal Society of Chemistry 2020

Table 1 The processed form and application of various COFs discussed in this review

COF	Processed form	Application	Ref.
Py-azine COF	Powder	Explosives detection	86
COF-BABD-BD, COF-BABD-BZ	Powder	Explosives detection	90
Py-TPE-COF	Nanospheres	Explosives detection	91
3D-Py-COF	Powder	Explosives detection	92
COF-LZU8	Powder	Hg^{2+} sensing	93
COF-JLU3	Powder	Cu^{2+} sensing	37
TaTa, DhaTab, TRITER-1, TzDa	Powder	Fe^{3+} sensing	94
Bth-Dha, Bth-Dma	Powder	Fe^{3+} sensing	95
TPE-Ph COF	Powder	Ammonia sensing	79
CCOF 7, CCOF 8	Nanosheets, membrane	Chirality sensing	96
COF-TpMA	Powder	Hydroxyl radical sensing, photo-degradation	97 and 106
TpTt	Powder	E–Z isomerization	38
TFPT-COF	Powder	H_2 evolution	98
BDT–ETTA COF	Thin film	H_2 evolution	59
N_3-COF	Powder	H_2 evolution	101
2D-COF-1	Powder	C–C bond forming	103
TTT-DTDA, TTT-BTDA	Powder	Radical polymerization	104
COF-JLU22	Powder	Dehalogenation	105
CuPor-Ph-COF	Hybrid composite	Photo-degradation	107
Tf-DHzDPr, Tf-DHzDM, TFPB-DHzDPr, Tf-DHzDM, TFPB-DHZDM, TFPB-DHzDS, TFPB-THz, TFPB-DHzDAll, DFDM-THz	Powder	White-light emission	89
TTA-DFP-COF	Powder	White-light emission	108
IISERP-COF7	Powder, thin film	White-light emission	77
3D-TPE-COF	Powder (in epoxy)	White-light emission	39
Py-tTII COF	Thin film	Photodetection	109
TpBpy	Powder	Thermometer	110

of not only powdered materials, but also thin films, nanosheets, and nanofibers. When processed into nanoparticles, COF-based chemical sensors for explosives can achieve sensitivities down to the ppb level. Other sensors are now available for metal ions, organic contaminants, and even hydroxyl radicals. By immobilizing chiral moieties onto the framework and then exfoliating into thin sheets, highly selective enantiomeric sensors can be fabricated into membranes for the detection of odor vapors.

Due to the photoactivity of the bulk system, COFs are also of great interest for photocatalysis. The band gaps of some systems are optimal for use in hydrogen evolution reactions and provide continuous hydrogen evolution, even in the case of one system's auto-exfoliation in its aqueous solution. COFs are also useful for photocatalyzing C–C bond forming reactions by aiding in processes such as radical initiation and SET, leading to improved radical polymerizations and drug derivatizations, respectively. In addition to molecule derivatizations, the degradation of toxic compounds has now been demonstrated with moderate to good conversions in relatively short timescales.

Multiple COF-based systems have been reported to achieve white-light emissions in solution and in the solid-state. Simultaneous emission of red, green, and blue light can be achieved *via* lanthanide doping or solvent variation to approach near-white-light emissions. These systems can also exhibit robust structural properties when coated on blue LEDs and illuminated for >1000 h, highlighting their potential as solid-state emitters for commercial applications.

Up to this point, a wide variety of luminescent COF systems have been introduced. However, because of the inconsistent and sometimes unpredictable nature of these materials, investigation into their fundamental properties remains a topic of interest. At present, it remains difficult to predict whether a COF architecture that includes a chromophore will yield a luminescent system, or if quenching phenomena will render it non-emissive. In addition, it has been observed that COF emissions can be completely quenched as a result of changing the covalent linkage. Therefore, there is a strong need for further investigation into quenching mechanisms and covalent linkage-dependent fluorescence in order to accurately predict the success of future system designs.

In addition to these challenges, at present, there are a limited number of building blocks available for luminescent COF synthesis, considering the vast number of well-studied chromophores. It is important to continue introducing new building blocks not only to modulate the architectural properties of the COF skeleton, but also to tune the luminescent behavior of the system. Similarly, expanding the scope of covalent linkages has shown great success in enabling the use of more complex functionalized building blocks in COF synthesis. With the new insights that have come from recent mechanistic investigations, it may be possible to synthesize even more complex frameworks with inherent functionality. Taken together, these advancements will allow for the intentional design of a vast range of photoactive systems, and therefore diversify the scope of their applications.

In summary, significant progress has been made towards understanding the translation from small-molecule luminescent behavior to 2D and 3D COF structures. As a direct result, emerging systems have demonstrated great potential in a wide variety of fields. However, close multidisciplinary collaboration between fields including biomedicine, chemical engineering,

and materials science should be encouraged for successful implementation of luminescent COF systems for practical applications.

Conflicts of interest

There are no conflicts to declare.

Acknowledgements

References

1 H. Zhu, C. C. Lin, W. Luo, S. Shu, Z. Liu, Y. Liu, J. Kong, E. Ma, Y. Cao, R.-S. Liu and X. Chen, *Nat. Commun.*, 2014, **5**, 4312.

2 Q. Zhang, B. Li, S. Huang, H. Nomura, H. Tanaka and C. Adachi, *Nat. Photonics*, 2014, **8**, 326.

3 C. Yang, D. Qi, J. Liang, X. Wang, F. Cao, Y. He, X. Ouyang, B. Zhu, W. Wen, T. Jia, J. Tian, L. Gao, Z. Sun, S. Zhang and L. V. Wang, *Laser Phys. Lett.*, 2018, **15**, 116202.

4 P. F. Jones, *Forensic Sci.*, American Chemical Society, 1975, ch. 19, vol. 13, pp. 183–196.

5 N. J. Turro, V. Ramamurthy and J. C. Scaiano, *Principles of Molecular Photochemistry – An Introduction*, University Science Books, USA, 2009.

6 Z. Pan, Y.-Y. Lu and F. Liu, *Nat. Mater.*, 2011, **11**, 58.

7 V. A. Davankov and M. P. Tsyurupa, *React. Polym.*, 1990, **13**, 27–42.

8 Y. Xu, L. Chen, Z. Guo, A. Nagai and D. Jiang, *J. Am. Chem. Soc.*, 2011, **133**, 17622–17625.

9 P. M. Budd, B. S. Ghanem, S. Makhseed, N. B. McKeown, K. J. Msayib and C. E. Tattershall, *Chem. Commun.*, 2004, 230–231.

10 M. Dressler, *J. Chromatogr. A*, 1979, **165**, 167–206.

11 P. Jagadesan, T. Whittemore, T. Beirl, C. Turro and P. L. McGrier, *Chem. – Eur. J.*, 2017, **23**, 917–925.

12 Y. Li, Y. He, F. Guo, S. Zhang, Y. Liu, W. P. Lustig, S. Bi, L. J. Williams, J. Hu and J. Li, *ACS Appl. Mater. Interfaces*, 2019, **11**, 27394–27401.

13 D. Chen, C. Liu, J. Tang, L. Luo and G. Yu, *Polym. Chem.*, 2019, **10**, 1168–1181.

14 K. Watanabe and K. Akagi, *Sci. Technol. Adv. Mater.*, 2014, **15**, 044203.

15 O. M. Yaghi, G. Li and H. Li, *Nature*, 1995, **378**, 703–706.

16 Y. Cui, Y. Yue, G. Qian and B. Chen, *Chem. Rev.*, 2012, **112**, 1126–1162.

17 A. Deshmukh, S. Bandyopadhyay, A. James and A. Patra, *J. Mater. Chem. C*, 2016, **4**, 4427–4433.

18 L. Chen, D. W. McBranch, H.-L. Wang, R. Helgeson, F. Wudl and D. G. Whitten, *Proc. Natl. Acad. Sci. U. S. A.*, 1999, **96**, 12287.

19 S. Bi, Y. Li, S. Zhang, J. Hu, L. Wang and H. Liu, *J. Mater. Chem. C*, 2018, **6**, 3961–3967.

20 P. Pallavi, S. Bandyopadhyay, J. Louis, A. Deshmukh and A. Patra, *Chem. Commun.*, 2017, **53**, 1257–1260.

21 C. Gu, Y. Chen, Z. Zhang, S. Xue, S. Sun, K. Zhang, C. Zhong, H. Zhang, Y. Pan, Y. Lv, Y. Yang, F. Li, S. Zhang, F. Huang and Y. Ma, *Adv. Mater.*, 2013, **25**, 3443–3448.

22 T. Mondal, S. Mondal, S. Bose, D. Sengupta, U. K. Ghorai and S. K. Saha, *J. Mater. Chem. C*, 2018, **6**, 614–621.

23 R. Chen, W.-C. Chen, L. Yan, S. Tian, B. Liu, X. Chen, C.-S. Lee and W. Zhang, *J. Mater. Chem. B*, 2019, **7**, 4763–4770.

24 G. Lan, K. Ni and W. Lin, *Coord. Chem. Rev.*, 2019, **379**, 65–81.

25 K. Lu, C. He and W. Lin, *J. Am. Chem. Soc.*, 2014, **136**, 16712–16715.

26 Z. Li, X. Feng, S. Gao, Y. Jin, W. Zhao, H. Liu, X. Yang, S. Hu, K. Cheng and J. Zhang, *ACS Appl. Bio Mater.*, 2019, **2**, 613–618.

27 A. P. Côté, A. I. Benin, N. W. Ockwig, M. Keeffe, A. J. Matzger and O. M. Yaghi, *Science*, 2005, **310**, 1166.

28 C. S. Diercks and O. M. Yaghi, *Science*, 2017, **355**, eaal1585.

29 X. Feng, X. Ding and D. Jiang, *Chem. Soc. Rev.*, 2012, **41**, 6010–6022.

30 C. R. Mulzer, L. Shen, R. P. Bisbey, J. R. McKone, N. Zhang, H. D. Abruña and W. R. Dichtel, *ACS Cent. Sci.*, 2016, **2**, 667–673.

31 F. Xu, S. Yang, X. Chen, Q. Liu, H. Li, H. Wang, B. Wei and D. Jiang, *Chem. Sci.*, 2019, **10**, 6001–6006.

32 Z.-J. Mu, X. Ding, Z.-Y. Chen and B.-H. Han, *ACS Appl. Mater. Interfaces*, 2018, **10**, 41350–41358.

33 X. Wu, X. Han, J. Zhang, H. Jiang, B. Hou, Y. Liu and Y. Cui, *Organometallics*, 2019, **38**, 3474–3479.

34 L. Zhu and Y.-B. Zhang, *Molecules*, 2017, **22**, 1149–1178.

35 D. A. Pyles, J. W. Crowe, L. A. Baldwin and P. L. McGrier, *ACS Macro Lett.*, 2016, **5**, 1055–1058.

36 C. R. DeBlase and W. R. Dichtel, *Macromolecules*, 2016, **49**, 5297–5305.

37 Z. Li, Y. Zhang, H. Xia, Y. Mu and X. Liu, *Chem. Commun.*, 2016, **52**, 6613–6616.

38 M. Bhadra, S. Kandambeth, M. K. Sahoo, M. Addicoat, E. Balaraman and R. Banerjee, *J. Am. Chem. Soc.*, 2019, **141**, 6152–6156.

39 H. Ding, J. Li, G. Xie, G. Lin, R. Chen, Z. Peng, C. Yang, B. Wang, J. Sun and C. Wang, *Nat. Commun.*, 2018, **9**, 5234.

40 F. J. Uribe-Romo, J. R. Hunt, H. Furukawa, C. Klöck, M. O'Keeffe and O. M. Yaghi, *J. Am. Chem. Soc.*, 2009, **131**, 4570–4571.

41 P. J. Waller, Y. S. AlFaraj, C. S. Diercks, N. N. Jarenwattananon and O. M. Yaghi, *J. Am. Chem. Soc.*, 2018, **140**, 9099–9103.

42 H. Lyu, C. S. Diercks, C. Zhu and O. M. Yaghi, *J. Am. Chem. Soc.*, 2019, **141**, 6848–6852.

43 H. M. El-Kaderi, J. R. Hunt, J. L. Mendoza-Cortés, A. P. Côté, R. E. Taylor, M. Keeffe and O. M. Yaghi, *Science*, 2007, **316**, 268.

44 L. A. Baldwin, J. W. Crowe, D. A. Pyles and P. L. McGrier, *J. Am. Chem. Soc.*, 2016, **138**, 15134–15137.

862 | *Chem. Soc. Rev.*, 2020, **49**, 839–864

This journal is © The Royal Society of Chemistry 2020

45 M. S. Lohse and T. Bein, *Adv. Funct. Mater.*, 2018, **28**, 1705553.

46 S. Kandambeth, K. Dey and R. Banerjee, *J. Am. Chem. Soc.*, 2019, **141**, 1807–1822.

47 D. Rodríguez-San-Miguel and F. Zamora, *Chem. Soc. Rev.*, 2019, **48**, 4375–4386.

48 D. Beaudoin, T. Maris and J. D. Wuest, *Nat. Chem.*, 2013, **5**, 830.

49 T. Ma, E. A. Kapustin, S. X. Yin, L. Liang, Z. Zhou, J. Niu, L.-H. Li, Y. Wang, J. Su, J. Li, X. Wang, W. D. Wang, W. Wang, J. Sun and O. M. Yaghi, *Science*, 2018, **361**, 48.

50 B. J. Smith and W. R. Dichtel, *J. Am. Chem. Soc.*, 2014, **136**, 8783–8789.

51 A. M. Evans, L. R. Parent, N. C. Flanders, R. P. Bisbey, E. Vitaku, M. S. Kirschner, R. D. Schaller, L. X. Chen, N. C. Gianneschi and W. R. Dichtel, *Science*, 2018, **361**, 52.

52 E. L. Spitler, B. T. Koo, J. L. Novotney, J. W. Colson, F. J. Uribe-Romo, G. D. Gutierrez, P. Clancy and W. R. Dichtel, *J. Am. Chem. Soc.*, 2011, **133**, 19416–19421.

53 C. R. DeBlase, K. Hernández-Burgos, K. E. Silberstein, G. G. Rodríguez-Calero, R. P. Bisbey, H. D. Abruña and W. R. Dichtel, *ACS Nano*, 2015, **9**, 3178–3183.

54 R. P. Bisbey, C. R. DeBlase, B. J. Smith and W. R. Dichtel, *J. Am. Chem. Soc.*, 2016, **138**, 11433–11436.

55 J. I. Feldblyum, C. H. McCreery, S. C. Andrews, T. Kurosawa, E. J. G. Santos, V. Duong, L. Fang, A. L. Ayzner and Z. Bao, *Chem. Commun.*, 2015, **51**, 13894–13897.

56 K. Dey, M. Pal, K. C. Rout, S. Kunjattu H, A. Das, R. Mukherjee, U. K. Kharul and R. Banerjee, *J. Am. Chem. Soc.*, 2017, **139**, 13083–13091.

57 J. W. Colson, A. R. Woll, A. Mukherjee, M. P. Levendorf, E. L. Spitler, V. B. Shields, M. G. Spencer, J. Park and W. R. Dichtel, *Science*, 2011, **332**, 228.

58 J. M. Rotter, S. Weinberger, J. Kampmann, T. Sick, M. Shalom, T. Bein and D. D. Medina, *Chem. Mater.*, 2019, **31**, 10008–10016.

59 T. Sick, A. G. Hufnagel, J. Kampmann, I. Kondofersky, M. Calik, J. M. Rotter, A. Evans, M. Döblinger, S. Herbert, K. Peters, D. Böhm, P. Knochel, D. D. Medina, D. Fattakhova-Rohlfing and T. Bein, *J. Am. Chem. Soc.*, 2018, **140**, 2085–2092.

60 D. D. Medina, M. L. Petrus, A. N. Jumabekov, J. T. Margraf, S. Weinberger, J. M. Rotter, T. Clark and T. Bein, *ACS Nano*, 2017, **11**, 2706–2713.

61 D. D. Medina, V. Werner, F. Auras, R. Tautz, M. Dogru, J. Schuster, S. Linke, M. Döblinger, J. Feldmann, P. Knochel and T. Bein, *ACS Nano*, 2014, **8**, 4042–4052.

62 C. E. Wayne and R. P. Wayne, *Photochemistry*, Oxford University Press, 1996.

63 Y. Yamaguchi, Y. Matsubara, T. Ochi, T. Wakamiya and Z.-I. Yoshida, *J. Am. Chem. Soc.*, 2008, **130**, 13867–13869.

64 L. Dou, Y. Liu, Z. Hong, G. Li and Y. Yang, *Chem. Rev.*, 2015, **115**, 12633–12665.

65 N. Huang, X. Ding, J. Kim, H. Ihee and D. Jiang, *Angew. Chem., Int. Ed.*, 2015, **54**, 8704–8707.

66 M. R. Rao, Y. Fang, S. De Feyter and D. F. Perepichka, *J. Am. Chem. Soc.*, 2017, **139**, 2421–2427.

67 X. Zhuang, W. Zhao, F. Zhang, Y. Cao, F. Liu, S. Bi and X. Feng, *Polym. Chem.*, 2016, **7**, 4176–4181.

68 S. Xu, G. Wang, B. P. Biswal, M. Addicoat, S. Paasch, W. Sheng, X. Zhuang, E. Brunner, T. Heine, R. Berger and X. Feng, *Angew. Chem., Int. Ed.*, 2019, **58**, 849–853.

69 E. Jin, M. Asada, Q. Xu, S. Dalapati, M. A. Addicoat, M. A. Brady, H. Xu, T. Nakamura, T. Heine, Q. Chen and D. Jiang, *Science*, 2017, **357**, 673–676.

70 Y. Zhao, H. Liu, C. Wu, Z. Zhang, Q. Pan, F. Hu, R. Wang, P. Li, X. Huang and Z. Li, *Angew. Chem., Int. Ed.*, 2019, **58**, 5376–5381.

71 E. Jin, J. Li, K. Geng, Q. Jiang, H. Xu, Q. Xu and D. Jiang, *Nat. Commun.*, 2018, **9**, 4143.

72 J. E. Kwon and S. Y. Park, *Adv. Mater.*, 2011, **23**, 3615–3642.

73 J. Zhao, S. Ji, Y. Chen, H. Guo and P. Yang, *Phys. Chem. Chem. Phys.*, 2012, **14**, 8803–8817.

74 V. S. Padalkar and S. Seki, *Chem. Soc. Rev.*, 2016, **45**, 169–202.

75 A. Weller, *Naturwissenschaften*, 1955, **42**, 175–176.

76 H.-L. Qian, C. Dai, C.-X. Yang and X.-P. Yan, *ACS Appl. Mater. Interfaces*, 2017, **9**, 24999–25005.

77 S. Haldar, D. Chakraborty, B. Roy, G. Banappanavar, K. Rinku, D. Mullangi, P. Hazra, D. Kabra and R. Vaidhyanathan, *J. Am. Chem. Soc.*, 2018, **140**, 13367–13374.

78 J. Mei, N. L. C. Leung, R. T. K. Kwok, J. W. Y. Lam and B. Z. Tang, *Chem. Rev.*, 2015, **115**, 11718–11940.

79 S. Dalapati, E. Jin, M. Addicoat, T. Heine and D. Jiang, *J. Am. Chem. Soc.*, 2016, **138**, 5797–5800.

80 J. Dong, X. Li, S. B. Peh, Y. D. Yuan, Y. Wang, D. Ji, S. Peng, G. Liu, S. Ying, D. Yuan, J. Jiang, S. Ramakrishna and D. Zhao, *Chem. Mater.*, 2019, **31**, 146–160.

81 S. Wan, J. Guo, J. Kim, H. Ihee and D. Jiang, *Angew. Chem., Int. Ed.*, 2008, **47**, 8826–8830.

82 S. Wan, J. Guo, J. Kim, H. Ihee and D. Jiang, *Angew. Chem., Int. Ed.*, 2009, **48**, 5439–5442.

83 F. Auras, L. Ascherl, A. H. Hakimioun, J. T. Margraf, F. C. Hanusch, S. Reuter, D. Bessinger, M. Döblinger, C. Hettstedt, K. Karaghiosoff, S. Herbert, P. Knochel, T. Clark and T. Bein, *J. Am. Chem. Soc.*, 2016, **138**, 16703–16710.

84 J. W. Crowe, L. A. Baldwin and P. L. McGrier, *J. Am. Chem. Soc.*, 2016, **138**, 10120–10123.

85 L. Stegbauer, S. Zech, G. Savasci, T. Banerjee, F. Podjaski, K. Schwinghammer, C. Ochsenfeld and B. V. Lotsch, *Adv. Energy Mater.*, 2018, **8**, 1703278.

86 S. Dalapati, S. Jin, J. Gao, Y. Xu, A. Nagai and D. Jiang, *J. Am. Chem. Soc.*, 2013, **135**, 17310–17313.

87 X. Chen, N. Huang, J. Gao, H. Xu, F. Xu and D. Jiang, *Chem. Commun.*, 2014, **50**, 6161–6163.

88 A. C. Pratt, *Chem. Soc. Rev.*, 1977, **6**, 63–81.

89 X. Li, Q. Gao, J. Wang, Y. Chen, Z.-H. Chen, H.-S. Xu, W. Tang, K. Leng, G.-H. Ning, J. Wu, Q.-H. Xu, S. Y. Quek, Y. Lu and K. P. Loh, *Nat. Commun.*, 2018, **9**, 2335.

90 M.-W. Zhu, S.-Q. Xu, X.-Z. Wang, Y. Chen, L. Dai and X. Zhao, *Chem. Commun.*, 2018, **54**, 2308–2311.

91 Q. Gao, X. Li, G.-H. Ning, K. Leng, B. Tian, C. Liu, W. Tang, H.-S. Xu and K. P. Loh, *Chem. Commun.*, 2018, **54**, 2349–2352.

This journal is © The Royal Society of Chemistry 2020

Chem. Soc. Rev., 2020, **49**, 839–864 | **863**

92 G. Lin, H. Ding, D. Yuan, B. Wang and C. Wang, *J. Am. Chem. Soc.*, 2016, **138**, 3302–3305.

93 S.-Y. Ding, M. Dong, Y.-W. Wang, Y.-T. Chen, H.-Z. Wang, C.-Y. Su and W. Wang, *J. Am. Chem. Soc.*, 2016, **138**, 3031–3037.

94 L.-L. Wang, C.-X. Yang and X.-P. Yan, *Sci. China: Chem.*, 2018, **61**, 1470–1474.

95 G. Chen, H.-H. Lan, S.-L. Cai, B. Sun, X.-L. Li, Z.-H. He, S.-R. Zheng, J. Fan, Y. Liu and W.-G. Zhang, *ACS Appl. Mater. Interfaces*, 2019, **11**, 12830–12837.

96 X. Wu, X. Han, Q. Xu, Y. Liu, C. Yuan, S. Yang, Y. Liu, J. Jiang and Y. Cui, *J. Am. Chem. Soc.*, 2019, **141**, 7081–7089.

97 W. Liu, Y. Cao, W. Wang, D. Gong, T. Cao, J. Qian, K. Iqbal, W. Qin and H. Guo, *Chem. Commun.*, 2019, **55**, 167–170.

98 L. Stegbauer, K. Schwinghammer and B. V. Lotsch, *Chem. Sci.*, 2014, **5**, 2789–2793.

99 R. van de Krol, Y. Liang and J. Schoonman, *J. Mater. Chem.*, 2008, **18**, 2311–2320.

100 T.-Y. Zhou, S.-Q. Xu, Q. Wen, Z.-F. Pang and X. Zhao, *J. Am. Chem. Soc.*, 2014, **136**, 15885–15888.

101 V. S. Vyas, F. Haase, L. Stegbauer, G. Savasci, F. Podjaski, C. Ochsenfeld and B. V. Lotsch, *Nat. Commun.*, 2015, **6**, 8508.

102 R. Ballini, S. Gabrielli and A. Palmieri, *Synlett*, 2009, 965–967.

103 M. Tian, S. Liu, X. Bu, J. Yu and X. Yang, *Chem. – Eur. J.*, 2020, **26**, 369–373.

104 P. Pachfule, A. Acharjya, J. Roeser, R. P. Sivasankaran, M.-Y. Ye, A. Brückner, J. Schmidt and A. Thomas, *Chem. Sci.*, 2019, **10**, 8316–8322.

105 Z. Li, Y. Zhi, P. Shao, H. Xia, G. Li, X. Feng, X. Chen, Z. Shi and X. Liu, *Appl. Catal., B*, 2019, **245**, 334–342.

106 H. Lv, X. Zhao, H. Niu, S. He, Z. Tang, F. Wu and J. P. Giesy, *J. Hazard. Mater.*, 2019, **369**, 494–502.

107 Y. Hou, C.-X. Cui, E. Zhang, J.-C. Wang, Y. Li, Y. Zhang, Y. Zhang, Q. Wang and J. Jiang, *Dalton Trans.*, 2019, **48**, 14989–14995.

108 C. Krishnaraj, A. M. Kaczmarek, H. S. Jena, K. Leus, N. Chaoui, J. Schmidt, R. Van Deun and P. Van Der Voort, *ACS Appl. Mater. Interfaces*, 2019, **11**, 27343–27352.

109 D. Bessinger, L. Ascherl, F. Auras and T. Bein, *J. Am. Chem. Soc.*, 2017, **139**, 12035–12042.

110 A. M. Kaczmrek, Y. Liu, M. K. Kaczmarek, A. H. Liu, L. D. Carlos and P. Van Der Voort, *Angew. Chem., Int. Ed.*, 2020, **59**, 2–11.